Leukemia-intrinsic determinants of CAR-T response revealed by *in vivo* genome-wide CRISPR screening

Azucena Ramos,[1,2†], Catherine E. Koch [1,2†], Yunpeng Liu,[1,2†] Riley D. Hellinger,[1] Taeyoon Kyung,[1,3] Rebecca C Larson,[8,9] Julia Fröse,[1] Daniel Goulet,[1] John G. Doench,[3] Aviv Regev,[2,4,5,6,7] Marcela V. Maus,[5,8,9,10] Michael E. Birnbaum,[1,3,8] Michael T. Hemann[1,2,4]*

[1]Koch Institute for Integrative Cancer Research, Massachusetts Institute of Technology, Cambridge, MA, USA

[2]Department of Biology, Massachusetts Institute of Technology, Cambridge, MA, USA

[3]Department of Biological Engineering, Massachusetts Institute of Technology, Cambridge, MA, USA.

[4]Ludwig Center for Cancer Research at MIT, Boston, MA, USA.

[5]Broad Institute of Harvard and Massachusetts Institute of Technology, Cambridge, Massachusetts 02142, USA

[6]Klarman Cell Observatory, Broad Institute of MIT and Harvard, Cambridge, MA, USA.

[7]Howard Hughes Medical Institute, Chevy Chase, MD, USA.

[8]Cellular Immunotherapy Program, Cancer Center, Department of Medicine, Massachusetts General Hospital, Boston, MA, USA.

[9]Immunology Program, Harvard Medical School, Boston, MA, USA.

[10]Ragon Institute of MIT, MGH, and Harvard, Cambridge, MA, USA.

† These authors contributed equally to this work

*Correspondence: hemann@mit.edu

Main Text

Abstract

CAR-T cells are a promising new treatment for B cell malignancies. However, the majority of patients inevitably go on to experience disease relapse through largely unknown means. To investigate leukemia-intrinsic CAR-T resistance mechanisms, we performed genome-wide CRISPR-Cas9 loss-of-function screening in an immunocompetent murine model of B cell acute lymphoblastic leukemia (B-ALL). We identified IFN**γ**/JAK/STAT signaling and components of the antigen processing and presentation pathway as key mediators of resistance to anti-CD19 CAR-T therapy *in vivo*, but not *in vitro*. Transcriptional characterization of this model demonstrated an upregulation of these pathways in CAR-T treated relapsed tumors, and examination of data from CAR-T treated B-ALL patients revealed an association between poor outcomes and increased expression of JAK/STAT/MHC-I in leukemia cells. Together, our data identify an unexpected mechanism of resistance to immunotherapy, in which tumor cell interaction with IFN**γ**-secreting CAR-T cells *in vivo* activates the expression of an MHC-I inhibitory T cell program.

Introduction

Immunotherapies have emerged as crucial components of cancer treatment and are quickly becoming the standard of care in a broad range of malignancies.[1] One of the most promising immunotherapy agents today is the adoptive cell transfer (ACT) of autologous T lymphocytes engineered to express chimeric antigen receptors (CARs).[2,3] Functionally, CARs redirect the cytotoxicity of immune cells towards a patient's tumor. Groundbreaking trials in relapsed B cell malignancies demonstrated extraordinary initial efficacy, with upwards of 90% of patients experiencing complete responses (CR).[4–8] Despite these impressive results, clinical data from CAR-T treated patients suggest that relapse is likely to be a significant and ongoing problem in this treatment modality. Recent studies have shown that while the median overall survival after CAR-T therapy is on the order of 12 to 20 months, upwards of 60% of patients will experience disease recurrence.[5,8–13] Further, up to 20% of B-ALL patients never achieve remission and applications to other $CD19^+$ B-cell malignancies such as chronic lymphocytic leukemia (CLL) and diffuse large B-cell lymphoma (DLBCL) have significantly lower CR rates.[5,8,11,14] Thus, gaining a more complete understanding of the factors governing response in CAR-T therapy may ultimately lead to improvements in CAR-T cell design or combination therapies that maintain remission and improve patient outcomes.

To date, a limited number of CAR-T resistance mechanisms have been reported in the
36 literature.[15] Treatment failure can be associated with loss of the infused CAR-T cell product, particularly in patients who never achieve remission.[16,17] This has led to the hypothesis that
38 CAR-T cell dysfunction is a central resistance mechanism in this treatment modality. Accordingly, significant efforts to characterize T cell dysfunction have been undertaken, and
40 factors such as the quality of harvested T-cells and variations in production and manufacturing have all been implicated. Leukemia-intrinsic changes have also been described, with target
42 antigen loss arguably garnering the most attention.[18,19] Overall, relapse with $CD19^{-}$ disease has been shown to occur in up to one in four patients experiencing treatment failure.[20,21] In the case
44 of anti-CD19 CAR-T therapy, tumor cell loss of CD19 has been found to occur via various mechanisms, including mutations in the CD19 locus, alternative splicing of CD19 mRNA, and
46 through lineage switching.[15] Decidedly less is known about the underlying drivers of relapse in $CD19^{+}$ disease. Here, CAR-T cell dysfunction has again been posited as a contributor to
48 treatment failure. However, it is presently unclear to what degree intrinsic CAR-T dysfunction drives relapse in these patients, or whether pre-existing or acquired tumor cell adaptations can
50 function to facilitate or incite CAR-T dysfunction, independent of CD19 status. Interestingly, recent reports support a role for the latter idea. For example, Singh and colleagues showed that
52 impaired death receptor signaling in tumor cells can lead to resistance by inducing CAR-T cell dysfunction.[22] Gene expression analysis of pre-CAR-T treated patient samples demonstrated
54 that pre-existing tumor cell expression profiles in the death receptor pathway differed between patients achieving CRs and those who never responded to CAR-T therapy. Strikingly, these pre-
56 existing expression profiles successfully predicted therapeutic outcomes in an independent patient cohort, suggesting that in some cases, CAR-T resistance may arise from pre-existing
58 tumor cell alterations. These data, along with the paucity of known resistance mechanisms outside of target antigen loss or CAR-T cell dysfunction, highlight the urgent need to carefully
60 examine the role of tumor cell alterations in CAR-T treatment failure.

To systematically investigate potential mechanisms of leukemia-intrinsic resistance to
62 CAR-T cells in an unbiased manner, we performed parallel whole genome *in vitro* and *in vivo* CRISPR/Cas9-mediated loss-of-function (LOF) screens for factors involved in response and
64 resistance to anti-CD19 CAR-T cell treatment in a transplantable, immunocompetent mouse model of *BCR-ABL*$^{+}$ B cell acute lymphoblastic leukemia (B-ALL).[23,24] We then compared our
66 top *in vivo*-specific hits with single cell expression analysis data of relapsed B-ALL cells after CAR-T treatment, and with published patient clinical data. The resulting data indicate that the
68 interactions between interferon gamma (IFN**γ**)-secreting CAR-T cells and tumor cells can

promote leukemia-specific alterations that can fuel relapse. These findings suggest an
70 "adaptive" resistance mechanism to cell-based immunotherapy and point to new possibilities for enhancing CAR-T cell efficacy without modifying existing CAR-T cell products.
72

Results

74 **A fully immunocompetent mouse model of BCR-ABL1$^+$ B-ALL enables parallel *in vivo* and *in vitro* genome-wide screens for CAR-T resistance**

76 Using an established mouse model of *BCR-ABL1*$^+$ B-ALL with a high engraftment rate in immunocompetent, syngeneic recipient mice, we engineered Cas9 expressing cells
78 (Supplemental Figure 1a) with high cutting efficiencies (Supplemental Figure 1b) to allow for unbiased genome-wide screens.[23–27] To determine if an *in vivo* screen for CAR-T resistance
80 using immunocompetent hosts was tractable, we examined *in vivo* growth in both wildtype (WT) and Cas9$^+$ cells, reasoning that if Cas9 expression induced any immunogenic barrier, this would
82 manifest as delayed growth kinetics over time. A luciferase$^+$ Cas9$^+$ clone (20.12), growth matched its WT parental line *in vitro* was transplanted into non-irradiated immunocompetent
84 male C57BL/6J (B6) mice. Compared to the WT parental line, no significant growth delays in Cas9$^+$ cells could be detected *in vivo*, in any hematopoietic organ assayed (Supplemental
86 Figure 1c). Parallel experiments were also performed in non-irradiated male B6 mice and immunocompromised NOD-SCID/IL2Rg$^{-/-}$ (NSG) mice. If Cas9 was immunogenic in recipient
88 mice, immunosuppressed NSG mice transplanted with Cas9$^+$ cells would have succumbed to disease faster than immunocompetent B6 mice transplanted with the same cells. However, no
90 differences in disease latency were observed in repeated experiments (Supplemental Figure 1d).

92 We then examined the ability of murine CAR-T cells to suppress tumor cell growth *in vivo*. As patients treated with CAR-T therapy undergo lymphodepletion with cyclophosphamide
94 or irradiation prior to therapy,[28–30] we first subjected recipient mice to an irradiation-based lymphodepletion protocol prior to tumor transplantation and subsequent CAR-T treatment. To
96 calibrate the dose of CAR-T cells, we performed a series of *in vivo* dosing experiments utilizing CD28-based 2nd generation murine CARs targeting murine CD19 (mCD19). Previous groups
98 utilizing a similar construct successfully suppressed disease with CAR-T dose ranges in the millions of cells ($5x10^6$ to $2x10^7$) per animal.[28,29,31] In our model, doses of $7x10^6$ to $1x10^7$ CAR-T
100 cells per animal, administered two days after the transplantation of $0.6x10^6$ B-ALL cells achieved significant dose-dependent life extension (Figure 1a). To simultaneously monitor
102 disease suppression in real time, we used leukemia cells engineered to express firefly

luciferase.[26] Bioluminescence imaging completed at multiple time points after ACT
104 demonstrated that anti-mCD19 CAR-T cells could significantly suppress disease over time
(Figure 1b-f).

106 To ensure CAR-T functionality, we conducted concurrent matched *in vitro* cytotoxicity
assays for each independent experiment and measured CAR-T expansion and IFN**γ** (a cytokine
108 released by T cells in proinflammatory conditions) in the resulting culture supernatant.
Interestingly, murine B-ALL cell numbers could be significantly reduced but never fully
110 eliminated *in vitro*, even at very high effector to target (E:T) ratios (Figure 1g). CAR-T cells also
induced a rapid and dramatic loss of the mCD19 target epitope on the surface of B-ALL cells
112 (Figure 1h), a phenotype that our results suggest is target antigen-independent and not a
unique feature of our murine B-ALL model (Supplementary Figure 1e). Importantly, while
114 antigen loss was a primary phenotype in our B-ALL cells, our cytotoxicity assays still resulted in
activated CAR-T cells that expanded (Figure 1i) and released significant IFN**γ** after being co-
116 cultured with cells expressing their target antigen (Figure 1j).

Our group has previously shown that this mouse model of B-ALL is highly amenable to
118 *in vivo* LOF screens.[25,26] Thus, we next sought to determine the CAR-T cell dose that would
adequately suppress disease in a pooled *in vivo* screening setting.[25,26] Irradiated B6 mice were
120 transplanted with B-ALL cells (clone 20.12), treated with varying amounts of CAR-T cell doses,
and monitored recipient mice using bioluminescence imaging. Animals were sacrificed at peak
122 disease suppression which occurred on or before day 3 after adoptive cell transfer (ACT) of
CAR T cells (Supplementary Figure 1f). Total disease burden, target tumor antigen expression,
124 and CAR-T expansion were assayed in various hematopoietic organs. We aimed for an 80-90%
disease suppression rate, as this significant but incomplete level of tumor cell reduction would
126 allow for identification of alterations that could sensitize tumor cells to therapy. For the bone
marrow compartment, this was accomplished using $1.5x10^7$ CAR-T cells, while splenic and
128 peripheral blood compartments only required a dose of $1x10^7$ CAR-T cells (Figure 1k). Relapsed
disease harvested from CAR-T treated animals consistently showed a striking dose-dependent
130 loss of mCD19 surface expression along with significant CAR-T engraftment in all organs
examined (Figure 1l-m), a consistent phenotype observed across all *in vivo* experiments. Given
132 that we also observe significant antigen loss and concomitant CAR-T cell persistence in
relapsed animals (Supplemental Figure 1g), we reasoned that this phenotype was due to
134 ongoing CAR-T surveillance. Indeed, when mCD19 negative leukemia cells were harvested
from relapsed mice and cultured *in vitro*, mCD19 expression was restored as CAR-T cells were
136 depleted from culture (Supplementary figure 1h-i). Notably, human data has demonstrated that

as many as half of all patients relapse with antigen negative disease. Thus, our system may
138 model the antigen loss and leukemia relapse seen following CAR-T therapy in a large proportion of patients.[5,9,32]
140

Unbiased CRISPR/Cas9-mediated screen identifies genes and pathways involved in *in vivo* resistance to anti-CD19 CAR-T therapy

Having established a mouse model of anti-CD19 CAR-T treatment response, we next
144 sought to develop a CRISPR/Cas9 library that would enable genome-wide *in vivo* screens across a broad range of tumor models with varying engraftment rates. We generated a custom
146 single guide (sgRNA) library cloned into an optimized lentiviral backbone (Figure 1n-o). The library is composed of 48 sub-pools, each targeting the protein coding regions of approximately
148 430 unique murine genes. Importantly, sub-pools can be used as stand-alone screening libraries, as each contains all requisite controls needed for a screen. Given the high tumor
150 engraftment rate in our B-ALL model, we were able to pool our 48 sub-pools into groups of eight, limiting our entire genome-wide *in vivo* and *in vitro* screens to six screens completed over
152 two experiments using our CD28-based 2nd generation murine CAR constructs (Figure 1p).

To query factors responsible for CAR-T resistance, we targeted 21,958 protein coding
154 genes and subjected cells to either anti-CD19 CAR-T therapy or control CAR-T cells (targeting anti-hEGFRvIII which is not expressed in mice or on our B-ALL model) *in vitro* or *in vivo*. The *in*
156 *vivo* arm of our screen followed the layout of our optimized dose finding experiments. We observed that relapsed CAR-T treated mice harbored both CD19-positive and -negative
158 disease, as well as persistent CAR-T cell populations in both the spleen and bone marrow (Supplementary Figure 2a and b, respectively). Concurrent with this *in vivo* screen, we
160 performed parallel *in vitro* screens at two effector to target (E:T) ratios. (Figure 1q). We then used high-throughput sequencing to quantify sgRNA representation in B-ALL cells harvested in
162 each experimental arm. Importantly, we were able to confirm that we achieved extensive coverage of every sgRNA library pool screened (Supplementary Figure 2c-d). To confirm that
164 our screen was able to effectively interrogate gene function while remaining unaffected by possible artifacts from Cas9-mediated DNA breakage, we quantified the enrichment and
166 depletion of sgRNAs in the control treatment group compared to pre-screen input samples. Indeed, sgRNAs targeting known essential genes significantly depleted in the control treatment
168 groups, whereas those targeting intergenic regions as well as non-targeting sgRNAs did not (Supplementary Figure 2e).

170 As expected, samples treated with anti-CD19 CAR-T therapy demonstrated patterns of sgRNA enrichment and depletion that were largely distinct from control treated groups
172 (Supplementary Figure 2f). To assess the genetic dependencies involved in the response of B-ALL cells to anti-CD19 CAR-T treatment, we compared the anti-CD19 CAR-T and control
174 treatment arms of the screen across each of the 6 pools (Figure 2a). These results were then aggregated to generate a genome-wide perturbation landscape of CAR-T treatment response
176 (Figure 2b-c). Within such a landscape, sgRNAs depleting in response to CAR-T treatment target genes that putatively mediate resistance to CAR-T therapy, whereas those that enrich
178 target genes that likely sensitize B-ALL cells to CAR-T therapy. Two central features support the biological relevance of our findings; first, sgRNAs targeting the *Cd19* locus are the top overall
180 enrichers (Figure 2b-e) and second, the magnitude of enrichment and depletion appears to be positively associated with the dosage of anti-CD19 CAR-T cells administered (i.e. the selective
182 pressure experienced by target cells) (Figure 2b, left and middle panels and Figure 2c). Importantly, a comparison of top hits in the *in vivo* and *in vitro* arms of our screen (Figure 2f)
184 showed little overlap between hits from these two arms, suggesting that a co-culture screen modality is incapable of capturing key *in vivo* mechanisms of CAR-T treatment resistance. In
186 fact, certain sgRNAs show the opposite behavior in each setting. For example, several top enrichers in the *in vitro* arms of the screen, such as sgRNAs targeting the IFN**γ** signaling
188 pathways members Janus kinase 2 (*Jak*2), signal transducer and activator of transcription proteins (*Stat1*), and interferon gamma receptor 1 (*Ifngr1*), are found to be depleted in the *in*
190 *vivo* arms (Figure 2d, e).

We next sought to determine whether pathways independent of target molecule (CD19)
192 expression were involved in resistance to CAR-T therapy. Using gene set enrichment analysis (GSEA), we found that several signaling and metabolic processes within the MSigDB hallmark
194 gene sets, such as the JAK/STAT/IL-6 signaling axis, PI3K/AKT pathway, and oxidative phosphorylation (OXPHOS) were enriched among genes that potentially mediate *resistance*
196 (Figure 2g, depleters, above dotted line). In contrast, some of these pathways are enriched among genes that potentially *sensitize* cells to therapy *in vitro* (Figure 2g, below dotted line).
198 Additionally, enrichment analysis of KEGG pathway terms (Figure 2h) showed that top depleters in the *in vivo* arms of our screen are enriched for processes such as tumor necrosis factor (TNF)
200 signaling, immune checkpoint signaling, and immune response against infectious diseases. Interestingly, the interferon gamma receptor 1 (IFNGR1) along with JAK/STAT/IL-6 signaling
202 pathway components, and the murine histocompatibility 2, T region locus 23 (H2-T23, also known as Qa-1^{b}) are components of multiple enriched pathways, suggesting that these genes

204 may be at the center of cellular response to CAR-T therapy *in vivo*. Indeed, sgRNAs against these genes are among the top *in vivo*-specific depleters (Figure 2d, e).

206

The IFNγ pathway promotes resistance to CAR-T therapy *in vivo*

208 To further validate our findings, and particularly, hits in the JAK/STAT/IFNγ pathway, we conducted parallel *in vivo* and *in vitro* competition experiments (Figure 3a-c and Supplementary 210 Figure 3a). Here, we used a new, independently generated Cas9-expressing cell line (RH62) from our parental B-ALL model with high cutting efficiency and matched *in vitro* growth kinetics 212 as our screened clone (Supplemental Figure 3b, c). We focused on genes that when lost, significantly depleted in the *in vivo* arms of our screen, as they could represent drug targets that, 214 when inhibited, might potentiate the effects of CAR-T therapy. Using competition assays that compare the relative growth of mixtures of isogenic knock out or control B-ALL cells both *in vitro* 216 and *in vivo*, we found that the proportion of cells null for *Ifngr1*, *Jak2*, or *Stat1* significantly depleted in both the marrow and spleens of mice treated with anti-CD19 CAR-T therapy (Figure 218 3b, c showing log-scale depletion). Notably, no growth differences were noted in mice transplanted with identical cell mixtures but treated with control CAR-T cells, indicating that this 220 phenotype is not driven by fitness defects imparted on cells that have lost these genes. Interestingly, parallel *in vitro* experiments again demonstrated the opposite result, with *Ifngr1*, 222 *Jak2*, or *Stat1* knock out cells significantly enriching in the context of anti-CD19 CAR-T therapy (Supplementary Figure 3a). Ultimately, similar to our screen findings, these data demonstrate 224 that loss of *Ifngr1*, *Jak2*, or *Stat1* sensitizes B-ALL cells to CAR-T therapy *in vivo* while promoting resistance *in vitro*.

226 To further validate our *in vivo* results, we generated pure populations of leukemic cells deficient in *Ifngr1*, *Jak2*, or *Stat1* (Supplementary Figure 3d). Consistent with our previous data, 228 mice transplanted with these cells demonstrated an enhanced response to CAR-T therapy, resulting in significantly increased survival (Figure 3d and Supplementary Figure 3e) and even 230 curative outcomes. Interestingly, a parallel experiment conducted in NSG animals demonstrated that tumors deficient in *Ifngr1* remain highly sensitized to CAR-T therapy (Figure 3e), indicating 232 that this sensitization phenotype is largely dependent on interactions between tumor and CAR-T cells. Thus, tumor cells can directly co-opt IFNγ signaling *in vivo* to resist killing by CAR-T cells 234 using a mechanism that is independent of other cellular components of the adaptive immune system. Conversely, CAR-T efficacy *in vitro* appears to be at least partially dependent on the 236 ability of tumor cells to sense IFNγ. Together, these data highlight the significant difference between *in vitro* and *in vivo* contexts and demonstrate the importance of investigating tumor cell

238 response to CAR-T therapy in a physiologically relevant setting. These results also highlight a central role for the JAK/STAT/IFN**γ** pathway in promoting resistance to CAR-T therapy in B-ALL.

240

Global targeting of JAK/STAT signaling does not enhance CAR-T therapy

242 Having established the JAK/STAT/IFN**γ** pathway as a key mediator of response to CAR-T therapy, we next explored whether global blocking of IFN**γ** *in vivo* could potentiate the effects 244 of CAR-T therapy. To this end, we administered blocking antibodies targeting IFN**γ** the day before ACT, and every 3 days thereafter (Figure 3f). Rather than enhancing antitumor effects, 246 blocking IFN**γ** in the context of anti-mCD19 CAR-T treatment abrogated the anti-tumor effects of CAR-T cells. Here, mice treated with anti-CD19 and anti-IFN**γ** antibody succumb to disease at 248 the same time as mice treated with control CAR-T cells and an isotype control antibody (Figure 3g and Supplementary Figure 3f). Identical results were obtained when animals were co-treated 250 with ruxolitinib and CAR-T therapy in a similar experiment (Figure 3h, i and Supplementary Figure 3g-m). These data are consistent with results from recent studies which show that 252 drugging CAR-T cells with JAK/STAT inhibitors or knocking out *Ifng* in CAR-T cells significantly impairs their ability to eliminate tumor cells *in vitro* and *in vivo*, respectively.[31,33] Thus, IFN**γ** is 254 indispensable for sustaining CAR-T cell cytotoxicity *in vivo*, resulting in the lack of a therapeutic window for targeting this cytokine directly to sensitize tumor cells to CAR-T cell killing.

256

***H2-T23* is an *in vivo*-specific mediator of resistance to CAR-T therapy**

258 We next sought to examine hits in our screen with known immune inhibitory functions and expression patterns that have been shown to be induced by IFN**γ**/JAK/STAT 260 proinflammatory signaling. One of the most promising factors fitting these criteria is the non-classical class I major histocompatibility complex (MHC-I) gene Histocompatibility 2, T region 262 locus 23 (*H2-T23*) encoding Qa-1^{b}, the murine homolog of human leukocyte antigen (HLA)-E.[34,35] HLA-E is the only known ligand of the CD94/NKG2A receptor which is expressed on the 264 surface of natural killer (NK) and CD8^{+} T cells.[36–40] Binding of NKG2A/CD94 to its ligand transmits a signal that inhibits the effector functions of NK and CD8^{+} T cells (Figure 4a).[38–42] 266 Recently, several groups have reported significant enhancement in the antitumor effects of immune checkpoint blockade (ICB) and cancer vaccines when combined with blockade of the 268 HLA-E-NKG2A axis, and early clinical trials have demonstrated encouraging results in a variety of cancers, including hematologic malignancies.[35,41–43] To explore the possibility that inhibition of 270 this axis could also potentiate the effects of CAR-T therapy *in vivo*, we set out to validate *H2-T23*, again using competition assays. As observed in the primary screen, loss of *H2-T23* in B-

272 ALL cells does not change the *in vitro* response to CAR-T therapy (Supplemental Figure 4a).
Remarkably, most animals bearing tumors partially transduced with sgRNAs against *H2-T23*
274 relapsed with bone marrow disease that was substantially CD19 positive after CAR-T therapy, a
phenotype that was not observed in any other set of CAR T experiments or any other mice
276 receiving the same CAR-T cells in parallel experiments (Figure 4b, c). Interestingly, this
phenotype also appears to be limited to the bone marrow, as relapsed disease in the spleen of
278 these mice was predominantly CD19 negative (Supplementary figure 4b, c).

To further examine the consequence of Qa-1^b loss on CAR-T response, we generated
280 pure populations of Qa-1^b null B-ALL lines by sorting for bulk sgRNA-bearing cells that could no
longer be induced to express Qa-1^b (Supplementary Figure 4d, e).[42] Consistent with our
282 previous results, Qa-1^b knockout tumors were sensitized to CAR-T therapy *in vivo*, leading to
significant life extension, including curative outcomes in fully immunocompetent animals (Figure
284 4c). Notably, immunodeficient NSG recipient mice bearing Qa-1^b-deficient tumors showed
extended survival in response to CAR-T therapy but, unlike B6 recipients, eventually relapsed,
286 suggesting that full CAR-T efficacy may require other cellular components of the adaptive
immune system. Finally, to investigate whether cells deficient in components of the
288 JAK/STAT/IFN**γ** pathway are also functionally null for Qa-1^b, we performed *in vitro* cytotoxicity
experiments. While control cells were fully capable of inducing dose-dependent expression of
290 Qa-1^b upon exposure to anti-CD19 CAR-T cells, isogenic cell lines deficient in *Stat1*, *Jak2*, or
Ifngr1 were completely blunted in their ability to express this molecule at all E:T ratios examined
292 (Figure 4d) or when these experiments were repeated using only recombinant IFN**γ**
(Supplementary Figure 4f). Together, our data highlight a role for the Qa-1^b/NKG2A/CD94 axis
294 in promoting resistance to CAR-T therapy via a mechanism that appears to depend on the
sensing of IFN**γ** by tumor cells and additional cellular components of the endogenous immune
296 system.

298 **A JAK/STAT/IFNγ program delineates cells refractory to anti-CD19 CAR-T therapy**

To further explore transcriptional programs driving B-ALL CAR-T resistance mechanisms
300 highlighted by our screen and validation experiments, we transcriptionally profiled B-ALL cells
after *in vivo* treatment with CAR-T cells. Principal component analysis of transcription profiles
302 using the most variable genes across samples showed a clear separation of animals treated
with anti-CD19 CAR-T cells from those treated with control anti-hEGFRvIII CAR-T cells (Figure
304 5a). Differential expression analysis showed that several genes involved in JAK/STAT signaling
and antigen processing and presentation pathways, including *Stat1*, *Irf1*, *Socs1*, and several

306 major histocompatibility complex (MHC) genes, are highly expressed in samples treated with anti-CD19 CAR-T therapy compared to those treated with control CAR-T cells (Figure 5b).
308 Interestingly, sgRNAs targeting these genes are also among the top depleters in the bone marrow or spleen in our *in vivo* screen, suggesting that these genes are part of an expression
310 program that may contribute to therapeutic resistance. Consistently, GSEA of Hallmark pathways highlighted interferon response, allograft rejection, MYC/2F targets, and
312 IL6/JAK/STAT3 signaling as top pathways enriched in samples treated with anti-CD19 CAR-T cells (Figure 2c).
314 Like other tumor types, B-ALL often displays a heterogeneous *in vivo* response to therapy. To dissect the *in vivo* transcriptional responses to anti-CD19 CAR-T therapy at a finer
316 resolution and pinpoint specific cell populations giving rise to relapse, we performed droplet-based single-cell transcriptome profiling on a total of 124,523 cells harvested from the bone
318 marrow and spleen of mice treated with anti-CD19 or control anti-hEGFRvIII CAR-T cells. Unsupervised clustering revealed 15 distinct cell populations as seen in the 2-dimensional
320 uniform manifold approximation and projection (UMAP) plots in Figure 5d (left panel). Cells from different treatment arms and tissues occupy distinct clusters (Figure 4d, right panel and
322 Supplementary Figure 5a). Notably, we did not observe loss of *Cd19* transcript expression in any sample (Supplementary Figure 5b, left panel), indicating that loss of CD19 surface
324 expression in this context is likely the result of post-translational regulation. Remarkably, a few clusters (2, 4, 5, and 7) are substantially enriched for cells from anti-CD19 CAR-T treatment
326 groups while being depleted of cells from the control treatment groups (Figure 5e). Consistent with our bulk RNAseq data, these clusters are marked by elevated expression of genes in the
328 IFN**γ** signaling and allograft rejection pathways, as well as MYC and E2F target sets (Figure 5f). Importantly, several signature genes in cluster 2 are also among the top depleters in our *in vivo*
330 screens. Figure 4g highlights the magnitude and pervasiveness of the expression of these genes across cell clusters. Additionally, clusters 4, 5, and 7 are enriched for genes involved in
332 oxidative phosphorylation (OXPHOS) and mTORC1 signaling pathways (Figure 5f). Cells in clusters 2 and 4, which contain mostly splenic disease from anti-CD19 CAR-T treated animals,
334 show widespread and high expression of *Stat1* and *H2-T23* (Figure 5g, h). Intriguingly, transporter associated with antigen processing (*Tap1*) is also over-expressed in these clusters
336 (Supplementary Figure 5b, right panel). Cluster 7, which is almost entirely made up of cells from anti-CD19 CAR-T treated bone marrow, is marked by a strong G2/M arrest phenotype (Figure 5f
338 and Supplementary Figure 5c) along with high expression of *H2-T23* and *Stat1* (Figure 5h). Transcription factor (TF) motif analysis of the regulatory regions of genes specifically up-

340 regulated in clusters 2, 4, 5 and 7 showed enrichment of motifs for critical TFs involved in interferon response, such as ETS family TFs, IRF8 and ELK4, with particularly strong
342 enrichment in clusters 2 and 4 (Supplementary Figure 5d).

Our single-cell expression data, taken together with results from our *in vivo* screen and
344 validation assays, further support the hypothesis that cross-talk between antigen processing and presentation, and interferon gamma signaling pathways underlie the cellular response to
346 anti-CD19 CAR-T therapy in B-ALL cells. Here, a subset of cells characterized by high expression of genes associated with these pathways may be responsible for therapeutic
348 resistance.

350 **High JAK/STAT signaling correlates with CAR-T resistance in humans**

Finally, to examine whether JAK/STAT signaling in tumor cells might also promote
352 resistance to CAR-T therapy in human B cell malignancies, we examined RNAseq data sets generated using pre-treatment bone marrow biopsy samples from B-ALL patients who received
354 CAR-T therapy.[22] Here, we generated a sensitizer signature from the overlap of our bone marrow depleting hits and reasoned that decreased expression of this signature should
356 correlate with better outcomes in patients since these genes represent novel resistance mediators to CAR-T therapy. In line with our prediction, patients who experience complete
358 responses (CRs) show significantly less expression of this sensitization signature compared to non-responders (NRs) (Figure 6a). To further examine these patient data, we also generated a
360 JAK/STAT/MHC-I resistance signature by overlapping the top depleters in our screen with the top overexpressed genes in tumor cell cluster 2 from our transcriptional analysis. Strikingly, this
362 resistance signature is correlated with poor outcomes in CAR-T treated patients, with NRs demonstrating significantly increased expression of our JAK/STAT/MHC-I gene set compared to
364 CRs (Figure 6b). Interestingly, these data are consistent with recent reports in large B cell lymphoma (LBCL) where high intratumoral interferon signaling is correlated with poor outcomes
366 after CAR-T treatment in patients.[44] Here, tumor cell expression of an interferon stimulated gene resistance signature (ISG.RS) associated with ICB resistance, is a strong predictor for CAR-T
368 treatment failure in LBCL.[45,46] Further examination of this signature in our model revealed that relapsed B-ALL cells with high IFN**γ** signaling after CAR-T failure were also enriched for
370 expression of the ISG.RS gene set (Figure 6c). Taken together, these data suggest that intratumoral JAK/STAT/IFN**γ** signaling, along with downstream antigen processing and
372 presentation pathways, may be key determinants of CAR-T response in human B-ALL (Figure 6d).

374

Discussion

376 Despite the immense therapeutic potential of CAR-T therapy, emerging long-term follow up data has highlighted that relapse is likely to be a significant problem for most patients treated 378 with CAR-T cells.[5,8–13] Using our screening platform, we identified and validated JAK/STAT/IFN**γ** signaling and components of the antigen processing and presentation machinery as critical *in* 380 *vivo* mediators of CAR-T resistance in B-ALL. Notably, loss of these pathways *in vitro* results in either the opposite phenotype, as with JAK/STAT/IFN**γ** signaling, or no phenotype at all, as with 382 the MHC-I molecule, Qa-1^b, highlighting the importance of assaying CAR-T function in immunocompetent models of disease. We also show that tumor cells that have lost the ability to 384 sense IFN**γ**, either via loss of *Ifngr1* or loss of critical downstream signaling components of this pathway are also functionally null for Qa-1^b. Hence, the mechanism by which JAK/STAT/IFN**γ** 386 signaling promotes CAR-T resistance in B-ALL is, at least in part, dependent on IFN**γ**-induced MHC-I expression. This result is particularly surprising, given that the functionality of CAR-T 388 cells was designed to be completely independent of antigen presentation pathways. Our data directly argue against this notion, highlighting instead a critical role for MHC-I signaling in 390 determining CAR-T response, potentially through the engagement of inhibitory receptors on CAR-T cells themselves or on other cellular components of the immune system, most notably, 392 NK cells, in the case of Qa-1^b.

Our results also suggest that the resistance mechanisms to CAR-T therapy are quite 394 distinct from those seen in response to anti-PD1/CTLA4 immune checkpoint inhibitor therapy. Indeed, *loss* of JAK/STAT/IFN**γ** signaling is an established resistance mechanism to checkpoint 396 therapy, as these agents require target cell MHC expression to promote T-cell mediated killing. For example, LOF mutations in the IFN**γ** receptor signaling molecules *JAK1*/2 or the HLA class I 398 molecule β-2-microglobulin (B2M) have been shown to render tumors refractory to immune checkpoint blockade (ICB).[47–50] The tumor cell strategy for CAR-T cell evasion evinced by our 400 data represents an unexpected form of therapeutic resistance, in which tumor cells are modified by the therapeutic agent, itself, to achieve a resistant state. Specifically, B-ALL sensing of IFN**γ** 402 in the proinflammatory microenvironment following CAR-T treatment leads to JAK/STAT mediated induction of factors that promote CAR-T resistance. This form of adaptive resistance 404 suggests that tumor-specific targeting of JAK/STAT signaling or key downstream pathways may render B-ALL tumors sensitive to CAR-T cells that persist in an activated state after relapse. 406 Furthermore, these data suggest that adaptation to CAR-T therapy may confer a collateral

sensitivity to immunotherapies that target tumor cells induced to express high levels of surface
408 MHC.

Lastly, our results also have implications for patient stratification in CAR-T therapy. We
410 show that elevated expression of a JAK/STAT/MHC-I signature in pre-treatment patient samples is associated with poor outcomes in CAR-T therapy, raising the possibility that this
412 transcriptional program may delineate a group of patients that harbor B-ALL tumors with some amount of intrinsic CAR-T resistance. Given our data, it is tempting to speculate that harboring
414 leukemia cells primed for effective IFN**γ** sensing and downstream signaling sets the stage for therapeutic failure after B-ALL cells are exposed to high levels of this cytokine in the
416 proinflammatory, CAR-T treated microenvironment. However, the generation and examination of larger data sets from patients receiving CAR-T therapy will be required to more fully examine
418 this hypothesis. Ultimately, our data highlight novel strategies that could be exploited for both design of improved CAR-T treatment regimens with preexisting CAR-T products, and for the
420 development of pre-treatment tumor biomarkers that better predict which patients are most likely to benefit from this promising immunotherapy.

422

Methods

424 **Pooled sgRNA screening**

A custom genome-wide library divided into 48 sub pools was generated in collaboration with the
426 Broad Institute's Genetic Perturbation Platform (GPP). In total, 97,336 unique guides targeting the protein coding regions of 21,958 unique murine genes with 4 sgRNAs each (plus control non-
428 targeting and intragenic cutting guides) were included. All protein coding murine genes were subdivided into 48 pools by their initial KEGG term (obtained using KEGG REST API in BioPython,
430 biopython.org), in a non-redundant manner. All four guides targeting the protein coding region of any given gene were kept together in the same pool. Using this approach, only 36% of protein-
432 coding genes could be classified into a KEGG pathway. Thus, the first 14 sub pools and part of sub pool 15 were filled by KEGG genes. All other genes were randomly distributed among the
434 remaining sub pools. Mouse essential genes (defined as orthologous mouse genes for the human essential gene set from Hart et al., 2015, 1530 genes; obtained from Ensembl Biomart) were
436 divided evenly across all pools. Guides against human *EGFRvIII*, human *CD22*, human *CD19*, and murine *Cd19* were included in the first pool.[51] Guides against olfactory genes (1,133 total)
438 were also distributed evenly amongst all sub pools. All 48 sub pools were cloned into a lentiviral pRDA-Crimson_170 vector (Figure 1o). To preserve library complexity, a minimum of 1000-fold
440 coverage of the sgRNA library was maintained at each *in vitro* step before the screen, and at a

minimum of 150-fold coverage (range: 153 to 203-fold coverage *in vivo*, all *in vitro* screens were
442 performed above 500x) was maintained in all screens completed. Pool A consisted of the first 8 sub pools and had a total of 15,308 sgRNAs targeting the protein coding regions of 3,648 unique
444 mouse genes. Pool B consisted of sub pools 9-16 and had a total of 15,147 sgRNAs targeting the protein coding regions of 3,648 unique mouse genes. Pool C consisted of sub pools 17-24 and
446 had a total of 15,258 sgRNAs targeting the protein coding regions of 3,648 unique mouse genes. Pool D consisted of sub pools 25-32 and had a total of 17,335 sgRNAs targeting the protein
448 coding regions of 3,648 unique mouse genes. Pool E consisted of sub pools 33-40 and had a total of 14,713 sgRNAs targeting the protein coding regions of 3,648 unique mouse genes. Pool
450 F consisted of sub pools 41-48 and had a total of 19,575 sgRNAs targeting the protein coding regions of 3,718 unique mouse genes. Cloned and sequenced plasmid pools, and viral
452 supernatant were generated by the Broad Institute's GPP.

454 For screens, $Cas9^+$ cells were thawed, recovered, and expanded for 5 days to ensure robust growth, and then tested for cutting efficiency to ensure high rates of editing efficiency.[27,52] After
456 cutting assays were completed, cells were expanded over three additional days and infected with sub pools. For each of the 48 sub pools, $6x10^7$ cells were spin-infected with predetermined
458 amounts of viral supernatant (determined using titration experiments, data not shown), such that 15-30% of all cells were infected (expressed E2-Crimson, and survived puromycin selection;
460 MOI<<1). The resulting cells were resuspended at a concentration of 10^6 cells/mL in virus-containing medium supplemented with 10 µg/mL polybrene (Sigma), divided into 6-well plates,
462 and centrifuged at 1000xg and 37°C for 1.5 hrs. Cells were then pooled into flasks and cultured overnight. Thirty-six hours later, cell density was adjusted to 10^6 cells/mL (and was never allowed
464 to go over $3x10^6$ cells/mL) and puromycin selection (2 µg/mL, Gibco, A1113803) was started. Cells were selected over two days and then spun out of puromycin-containing medium. Cells were
466 then allowed to recover for one day, after which the appropriate number of infected, selected, and recovered cells were flow cytometry sorted and combined into their respective pools. The next
468 day, cells from large, combined pools were prepared for tail vein injection into mice or kept in culture for the *in vitro* screens. Two days later, CAR-T cells were adoptively transplanted into mice
470 via tail vein injection at the indicated doses. For all *in vitro* screens, $1.4x10^7$ library cells were seeded and treated two days later (on the same schedule as mice) with control CAR-T cells (anti-
472 hEGFRvIII), anti-mCD19 CAR-T cells, or with no CAR-T cells, at E:T ratios indicated in the text. *In vitro* CAR-T screens were set up in triplicate while the no CAR-T condition was kept in a single
474 plate. Input samples were collected just after puromycin selection had completed (Input PS) and

on the day cells were injected into mice/set up for *in vitro* screens (Input or Input DOI). Upon
476 becoming moribund, mice were sacrificed and E2-Crimson$^+$ cells were sorted from the bone marrow and spleen (average number sorted cells per compartment = 1.38×10^7). For *in vitro*
478 screens where the B-ALL cells viability was above 95% and represented more than 99% of all cells present in the sample, cells were counted and 2×10^7 cells were collected for gDNA isolation.
480 The only condition that did not meet this cutoff was the anti-mCD19 at E:T of 1:2 for all 6 pools. Here, CAR-T cells were completely gone from culture, but B-ALL viability of cells remained low at
482 30-60% across replicates, necessitating sorting to isolate cells ($1.4\text{-}2.0 \times 10^7$ sorted per replicate, per condition).

484

Finally, gDNA from all cells were isolated using the Machery Nagel L Midi NucleoSpin Blood Kit
486 (Clontech, 740954.20). Modifications to the manufacturer's instructions were added as follows: in step 1, cells were lysed in the kit's proteinase K containing lysis buffer for longer (overnight at
488 70°C). The next morning, lysates were allowed to cool to room temperature, 4.1 µL of RNase A (20 mg/mL; Clontech, 740505) was added, and cells were incubated for 5 minutes at room
490 temperature. The procedure then continued as indicated by the manufacturer. PCR inhibitors were removed from the resulting gDNA (Zymo Research, D6030) and the concentration of the
492 resulting gDNA was measured using the Qubit dsDNA HS assay kit (ThermoFisher, Q32854), and if necessary, diluted to 200 ng/µL with elution buffer. gDNA was then submitted for Illumina
494 sequencing.

496 **Screen hit discovery**

Sample quality control was performed by counting the number of gRNA sequences that show at
498 least 30 reads in each sample. Samples with more than 30% of gRNA sequences that were filtered out after the above procedure were excluded from further analyses. Guide RNA-level read
500 counts were scaled by total read count for each sample and logarithm-transformed. Gene-level enrichment and depletion scores were computed by averaging log-normalized read counts across
502 all gRNA sequences against each gene. Six different pooled libraries were aggregated targeting a total of 21,958 unique murine genes with a total of 88,793 sgRNAs (4 per gene plus non-
504 targeting and intergenic-cutting controls). Input samples were used as a baseline for computing scores. Specifically, every gene was first assigned an 'essentiality score' computed as the
506 difference (i.e. log-fold change) between the average gene-level counts for the gene across replicates and that in the input sample. The CAR-T therapy enrichment/depletion score for a given
508 gene is computed as the difference between the essentiality scores of that gene in anti-mCD19

CAR-T cell treated samples and in anti-hEGFRvIII CAR-T cell treated samples. For sample
510 groups that have at least 2 samples retained after quality control, Student's t-tests were performed to obtain p-values for assessing significance of difference between the scores in the treatment
512 group and the control group.

514 **Bulk transcriptome profiling and analysis**

Total RNA was extracted from $1x10^6$ cells per sample using the Macherey-Nagel Nucleospin
516 RNA Plus kit, and RNA sample quantity and quality was confirmed using an Agilent Fragment Analyzer. RNAseq libraries were created from 250ng of total RNA using the NEBNext UltraII
518 Directional RNA Library Prep kit (New England Biolabs) using half volume reagents and 14 cycles of PCR. Illumina library quality was confirmed using the Fragment Analyzer and qPCR and
520 sequenced on an Illumina NextSeq500 using v2.1 chemistry with 40nt paired end reads (RTA version 2.11.3). Paired-end RNA-seq data was used to quantify transcripts from the mm10 mouse
522 assembly with the Ensembl version 101 annotation using Salmon version 1.3.0.[53] Gene level summaries were prepared using tximport version 1.18.0[54] running under R version 4.0.3.[45]

524

Single cell transcriptome profiling and data processing

526 Mice were transplanted with $3x10^6$ B-ALL cells and challenged with 10^7 CAR-T cells targeting either CD19 or a control epitope (human EGFRvIII). Upon becoming moribund, mice were
528 sacrificed and B-ALL cells were sorted from the bone marrow and spleen. For each sample, approximately 10,000 live B-ALL cells were sorted for transcriptional profiling. Single-cell
530 expression libraries were prepared using the 10x Genomics Chromium v3 reagents. Sequencing data was aligned to the mm10 reference genome and converted to fastq files using bcl2fastq
532 (v2.20.0.422). Cell count matrices were generated using cellranger (v.5.0). Matrices were analyzed by Seurat (v4.0.4) for R (v4.0.2). Digital gene expression matrices were filtered to
534 exclude low quality cells (< 1000 UMI, < 400 genes or > 8000 genes, > 50% mitochondrial reads). Low-quality cells were further filtered from the dataset using the variance sink method as
536 previously described.[55] Briefly, data was normalized and scaled, known cell cycle genes were regressed out.[56] Principal component analysis was performed on regressed and scaled data.
538 Standard deviation of principal components was quantified using an elbow plot, input dimensions for SNN clustering (EGFRv3 bone marrow = 35, EGFRv3 spleen = 42, CD19 bone marrow = 30,
540 CD19 spleen = 30) at which standard deviation = 2. SNN clustering was performed to generate UMAP plots (k.param = 40, res = 0.5). Clusters containing low quality cells (50% of cells with >
542 10% mitochondrial reads) were removed from the dataset. After filtering, samples from bone

marrow and spleen treated with EGFRv3-CAR-T or CD19-CAR-T were merged into a single
544 dataset. Cell cycle phase was assigned using the cell cycle scoring function based on expression of known cell cycle genes.[56] Merged data set was normalized and scaled, cell cycle genes were
546 regressed out. Principal component analysis was performed, and standard deviation of principal components was quantified by elbow plot. Nearest neighbors were found (dim = 50, k.param =
548 40) then clustered using SNN clustering (res = 0.5). Enriched genes for each cluster were identified with the cluster marker function. Cluster occupancy was quantified for each treatment
550 condition and phase of the cell cycle to further define therapeutic response.

552 **Mouse maintenance and studies**

All mouse experiments were conducted under IUCAC-approved animal protocols at the
554 Massachusetts Institute of Technology. The mouse strains used in this study included C57BL/6 (Jackson) and NOD/SCID/IL2Rg$^{-/-}$ (NSG; Jackson Laboratory). Immunocompetent recipient mice
556 were sub-lethally irradiated (1 x 5 Gy) immediately prior to transplantation with B-ALL cells, receiving ACT of CAR-T cells 2 days later, as noted in the text. For *in vivo* screens, mice were
558 injected with 3x10^6 Cas9$^+$ library B-ALL cells and the indicated number of CAR-T cells. Both B-ALL and CAR-T cells were prepared for transplantation by resuspending in 200 µL Hank's
560 balanced salt solution (Lonza) and loaded in 27.5-gauge syringes (Becton Dickinson). All cell solutions were administered via tail vein injections. For *in vivo* blocking of IFN**γ**, mice were injected
562 i.p. every third day with 200µg of InVivoMAb anti-mouse IFN**γ** antibody (clone XMG1.2, Bio X Cell) or 200µg of InVivoMAb anti-horseradish peroxidase control antibody (clone HRPN, Bio X
564 Cell), starting the day after ACT. For *in vivo* inhibition of JAK1/2, Ruxolitinib (Selleckchem, INCB018424) was resuspended according to manufacturer guidelines and mice were dosed
566 every twelve hours via oral gavage with 90 mg/kg Ruxolitinib or vehicle control, starting the day after disease transplantation.

568

Bioluminescence studies

570 XenoLight D-Luciferin Potassium Salt D (PerkinElmer, 122799) was used for standard bioluminescent imaging (resuspended at 30 mg/mL in saline, sterile filtered, and stored at -80°C).
572 Mice were weighed and luciferin was loaded in 27.5-gauge syringes (Becton Dickinson) and administered via intraperitoneal injection at a dose of 165 mg/kg. Mice were then anesthetized
574 with 2.5% isoflurane (Piramal Critical Care, NDC# 66794-013-25), delivered at 1 L per minute in O_2. Ten minutes from the time of luciferin injection, animals were imaged on a Xenogen IVIS
576 system at consistent exposures between groups with small binning. Data was analyzed using

Living Image version 4.4 software (Caliper Life Sciences). Images were normalized to the same
578 color scale for figure generation.

580 **Cell culture**

All cell lines were mycoplasma negative.

582 Murine B-ALL cells: Cells were cultured in RPMI with L-glutamine (Corning, 10-040-CM), supplemented with 10% fetal bovine serum and 2-mercaptoethanol to a final concentration of
584 0.05mM (Gibco, 21985023).

Murine B-cell lymphoma cells (Eμ-Myc): Cells were cultured in medium composed of a 50:50 mix
586 of IMDM with L-glutamine and 25mM HEPES (Corning, 10-016-CM) and DMEM with L-glutamine and sodium pyruvate (Corning, 10-013-CM), supplemented with 10% FBS and 2-
588 mercaptoethanol to a final concentration of 0.05mM (Gibco, 21985023).

Murine T cells: T cells harvested from the spleens of mice were cultured in plates coated with
590 activating antibodies (as described in CAR-T cell production methods) in T cell medium (TCM): RPMI with L-glutamine (Corning, 10-040-CM), supplemented with 10% FBS, recombinant human
592 IL-2 (rhIL-2, final concentration of 20 ng/mL; Peprotech, Cat# 200-02-1mg), and 2-mercaptoethanol to a final concentration of 0.05mM (Gibco, 21985023).

594 Human cell lines: 293T and Raji cells were all mycoplasma negative. 293T cells are cultured in DMEM with L-glutamine and sodium pyruvate (Corning, 10-013-CM) supplemented with 10%
596 FBS. Raji cells were cultured in RPMI with L-glutamine (Corning, 10-040-CM) supplemented with 10% FBS.

598

Viral supernatant production

600 Viral supernatant was produced using standard methods. Briefly, 293T cells were transfected with retroviral or lentiviral transfer plasmid and packaging vector (retrovirus: pCL-Eco, Addgene,
602 12371; lentivirus: psPAX2, Addgene, 12260 with VSVg envelop plasmid pMD2.G, Addgene, 12259) using Mirus TransIT-LT1 (Mirus, MIR2305) as indicated by the manufacturer. The next
604 day, 293T cells were switched into medium composed of 60% RPMI complete and 40% DMEM complete. Viral supernatant was collected 24 and 48 hours after transfection, passed through a
606 0.45um filter to remove residual 293T cells, and kept at 4°C for a maximum of 4 days.

608 ***In vitro* killing assay**

In vitro CAR-T killing assays were performed using standard methods.[57,58] Briefly, target cells are
610 counted and co-cultured with or without CAR-T cells at indicated E:T ratios (accounting for CAR-

T infection rate) in RPMI complete supplemented with 2-mercaptoethanol and 10% FBS but no
612 rhIL-2. Sixteen to twenty-four hours later, the total cell number per well was counted and the cell suspension was analyzed by flow cytometry to assess for live/dead, %mCD19$^+$ cells, and %CD8$^+$
614 cells. The densities of each cell type (CAR-T, target cell, non-transduced T cell) were also determined via flow cytometry. The resulting target cell densities in CAR-T containing wells are
616 then normalized to the resulting target cell density in control wells seeded with the same number of target cells but without CAR-T cells.
618

Interferon gamma ELISA release assay

620 Standard methods were used for enzyme-linked immunosorbent assay (ELISA). Briefly, supernatant from *in vitro* CAR-T killing assays was collected and spun down to remove any
622 contaminating cells. IFN**γ** released into the supernatant by CAR-T cells is then measured using the DuoSet ELISA kit for mouse IFN**γ** (R&D systems, DY485) and Nunc MaxiSorp flat bottom
624 plates (Thermo Fisher Scientific, 44-2404-21) on a Tecan infinite 200 Pro machine, as indicated by the manufacturer. To ensure that the assay is completed within the linear range of the kit,
626 supernatant is initially diluted 1:10 in reagent diluent. At least six serial 4-fold dilutions are then performed. At least one standard curve for this assay is generated per plate and at least two
628 standard curves for the entire experiment are constructed using standard solutions supplied by the manufacturer. Substrate solution used is 1-Step™ Ultra TMB-ELISA (Thermo Fisher
630 Scientific, 34028) and stop solution used is sulfuric acid 2N stop solution (VWR, BDH7500-1). Bovine serum albumin (BSA; Sigma, A8022-500G) is prepared as a sterile filtered 5% stock in
632 PBS (Corning, 21-031-CV).

634 **CAR-T cell production**

Before collecting T cells, 6-well plates were coated overnight with activating antibodies against
636 mCD3e (Bio X-Cell, BE0001-1) and mCD28 (Bio X-Cell, BE0015-1) at 5 µg/mL each in PBS (Corning, 21-031-CV) at 4°C. The next day, 8–12-week-old male C57BL/6 mice (Jackson) were
638 sacrificed, and their spleens were collected. CD8$^+$ T cells were isolated using Miltenyi Biotec CD8a (Ly-2) MicroBeads for mouse (positive selection kit; Miltenyi, 130-117-044) and LS columns
640 (Miltenyi, Cat# 130-042-401) as indicated by the manufacturer. Coated plates were rinsed once with PBS and T cells were resuspended at 0.5×10^6 to 10^6 cells/mL in T cell medium (TCM, recipe
642 in cell culture methods). After 24 hours, activated T cells were collected and placed into fresh TCM after counting. Cell concentrations were then adjusted to 10^6 cells/mL in a 50:50 mix of
644 TCM:retroviral (RV) supernatant supplemented with protamine sulfate to a final concentration of

10 µg/mL (MS Biomedicals, ICN19472910), 2-mercaptoethanol to a final concentration of 0.05
646 mM, and rhIL-2 to a final concentration of 20 ng/mL. Once resupended, cells were spin-infected at 1000xg for 1.5 hrs at 37°C on new antibody coated plates. The next day, T cells were collected
648 from plates, resuspended in fresh TCM at a cell density of $0.5x10^6$ to 10^6 cells/mL, and re-plated on new antibody-coated plates. Twenty-four hours later, T cells were collected from antibody
650 coated plates and prepared for tail vein injection into animals or for *in vitro* kill assays/screens, as described above. T cells were always cultured and infected on PBS rinsed, antibody-coated 6-
652 well plates, as described above, except during *in vitro* killing assays where no activating antibodies were ever used.

654

Western Blotting

656 Cells were lysed with RIPA buffer (Boston BioProducts, BP-115) supplemented with 1X protease inhibitor mix (cOmplete EDTA-free, 11873580001, Roche). Protein concentration of cell lysates
658 was determined using Pierce BCA Protein Assay (ThermoFisher Scientific, 23225). Total protein (40-60µg) was separated on 4-12% Bis-Tris gradient SDS-PAGE gels (Life Technologies) and
660 then transferred to PVDF membranes (IPVH00010, EMD Millipore) for blotting.

662 **Plasmids, cloning, and sgRNAs**

<u>Packaging and envelope plasmids used for viral production</u>

664 Retrovirus: pCL-Eco (Addgene, 12371)

Lentivirus: psPAX2 (Addgene, 12260) with VSVg envelop plasmid pMD2.G (Addgene, 12259) or
666 pCMV-EcoEnv (Addgene, 15802)

<u>Chimeric Antigen Receptor (CAR) plasmids</u>

668 The murine CD19 targeting second generation CAR 1D3-28Z.1-3 containing inactivating mutations in the 1st and 3rd ITAM regions of the CD3-ζ chain was synthesized by Twist Bioscience
670 and cloned into the GFP^+ MP71 retroviral vector.[28,59] The clinically used scFv sequence (heavy chain linked to light chain variable regions) against human CD19, FMC63, was provided by the
672 Maus lab. A CD28-containing 2nd generation murine CAR targeting hCD19 protein was then constructed by switching out the scFv for 1D3-28Z.1-3 in the anti-mCD19 CAR and replacing it
674 with the FMC63 scFv (Twist Bioscience). The same technique was used for the 3C10 scFv targeting human EGFRvIII, which was reported by the Rosenberg lab.[60] All CAR constructs are
676 identical, containing a CD8a leader sequence, followed by the respective scFv, followed by an IgG4 hinge sequence, a portion of the murine CD28 molecule from amino acids IEFMY to the 3′
678 terminus, and finally, the cytoplasmic region of the murine CD3-ζ chain from amino acids RAKFS

to the 3′ terminus with both tyrosines in ITAMs 1 and 3 mutated to phenylalanines as described
680 (all in frame).[28] All CAR constructs were extensively tested to ensure that they only targeted their peptide of interest. Human EGFRvIII expression was induced using pMSCV-XZ066-EGFRvIII
682 (Addgene, plasmid 20737) and murine hEGFRvIII$^+$ B-ALL cells were generated. Retroviral supernatant to induce hCD19 expression was provided by the Maus lab. All CARs were
684 extensively tested *in vitro* (killing assays methods) and *in vivo* (as described in text) to ensure no off-target effects were present.

686 CRISPR plasmids

To generate Cas9$^+$ murine B-ALL cell lines, lentiCas9-Blast (Addgene, 52962) was used, and
688 cells were selected with Blasticidin (Gibco, A1113903) at 20 µg/mL for 7 days and then single cell cloned and assayed for Cas9 expression via WB. Guide RNAs for murine *Cd19* were designed
690 using the Broad Institute's sgRNA Designer tool (https://portals.broadinstitute.org/gppx/crispick/public) and cloned into lentiGuide-Puro (Addgene,
692 52963) for the functional cut assay (tracking loss of mCD19 on the cell surface) or pRDA-Crimson_170 to generate KOs of various test genes (vector testing, data not shown).[27] Guide
694 RNAs used are below (Forward/Reverse):

Murine *Cd19* sgRNAs:

696 sgRNA#42, targets exon 6 (5'-CACCGAATGACTGACCCCGCCAGG)/(5'-AAACCCTGGCGGGGTCAGTCATTC)

698 sgRNA#43, targets exon 2 (5'-CACCGCAATGTCTCAGACCATATGG)/(5'-AAACCCATATGGTCTGAGACATTGC)

700 Other plasmids

MSCV-mCherry (Addgene, 52114) was used to generate 20.12DP cells from mCherry$^-$ GFP$^+$
702 20.12 cells.

704 **Generating Qa-1^b knockout B-ALL cells**

B-ALL cell lines deficient for Qa-1^b were generated using CRISPR-Cas9 technology. Single guide
706 RNAs directed against the *H2-T23* locus were designed using the Broad Institute's sgRNA Designer tool and the sgRNA sequence (5'-GTACTACAATCAGAGTAACGA-3') was cloned into
708 pRDA-Crimson_170, as described above. Cas9$^+$ B-ALL cells (clone RH62) were transduced with sgRNAs and selected with puromycin over 48 hours. Loss of Qa-1^b was confirmed by incubating
710 transduced cells with 30 IU/mL IFN**γ** for 24 hours and subsequently analyzing Qa-1^b surface expression by flow cytometry, as previously described.[42] Qa-1b$^-$ cells were then FACS sorted
712 twice until a pure population of Qa-1^b knockout cells was established.

714 **Antibodies**

Western blotting: anti-β-ACTIN (Cell signaling, 4967S), anti-CD19 (Abcam, ab25232), anti-Cas9
716 (ActiveMotif, 61577), anti-JAK2 (Cell Signaling Technology, 3230), anti-IFNγR1/CD119 (R&D Systems, MAB10261), anti-STAT1 (Cell Signaling Technology, 9172), anti-rabbit IgG HRP-linked
718 antibody (Cell Signaling Technology, 7074), anti-mouse IgG HRP-linked antibody (Cell Signaling Technology, 7076), anti-rat IgG HRP-linked antibody (Cell Signaling Technology, 7077), Rabbit
720 anti-Armenian Hamster IgG H&L (HRP) (Abcam, ab5745).

722 Flow cytometry: anti-mouse CD19-BV785 (BioLegend, 115543), anti-mouse CD8-PE/Cy7 (BioLegend, 100722), anti-human CD19-APC/Cy7 (BioLegend, Cat# 302218), anti-mouse Qa-1^{b}-
724 BV786 (BD Biosciences, 744390).

726 **Statistical analysis**

All Statistical analyses were performed using GraphPad Prism 9 (GraphPad Software Inc). The
728 specific statistical tests performed are specified in figure legends. Differences are considered significant for P-values ≤ 0.05, or as indicated when adjustments for multiple hypothesis testing
730 was required.

732 **Data Availability**

RNA sequencing data generated in this manuscript is in the process of being uploaded to
734 publicly accessible online repositories. Sequencing data from all screens are available from the corresponding author on reasonable request. All other data are included within the manuscript
736 figures or as supplementary information.

738 **Acknowledgements**

The authors thank Hojun Li, Khloe Gordon, and members of the Hemann and Vander Heiden
740 labs for valuable discussions and intellectual input, the Koch Institute's Robert A. Swanson (1969) Biotechnology Center for technical support, specifically the Flow Cytometry and
742 Preclinical Imaging and Testing facilities, and S. Levine from the MIT BioMicro Center for informative discussions about guide library and scRNA sequencing. The authors also thank
744 Beatrice Grauman-Boss for her support generating CAR virus. This work was generously supported by the MIT Center for Precision Cancer Medicine, the Ludwig Center at MIT, a
746 Margaret A. Cunningham Immune Mechanisms in Cancer Research Fellowship, a David H.

Koch Graduate Fellowship, and the Paul and Daisy Soros Fellowship for New Americans. This
748 work was also supported in part by NCI R01-CA233477, R01-CA226898 and NIH/NIAID
R21AI151827 to M.T. Hemann and the Koch Institute Support (core) Grant P30-CA14051 from
750 the NCI.

752 **Author information**

Please note that Aviv Regev's initials are noted below as AV to differentiate them from those of
754 *co-author Azucena Ramos.*

Contributions

756 AR, YL, and MTH conceived the idea for the study. AR, YL, CK, and MTH designed the study.
AR, YL, CK, RH, and JF conducted experiments. RH provided support with characterization of
758 clone 20.12 and clone RH62, and the entirety of the screens. RCL provided support generating
clone 20.12. TK and RCL provided critical support in designing the CAR constructs. TK cloned
760 all CAR constructs. YL and DG analyzed scRNAseq data. AV, JGD, MM, and MEB gave vital
advice and provided reagents. AR and YL wrote the manuscript. All authors reviewed and
762 edited the manuscript.

764 Corresponding author: Michael T. Hemann – hemann@mit.edu

766 Figure 1

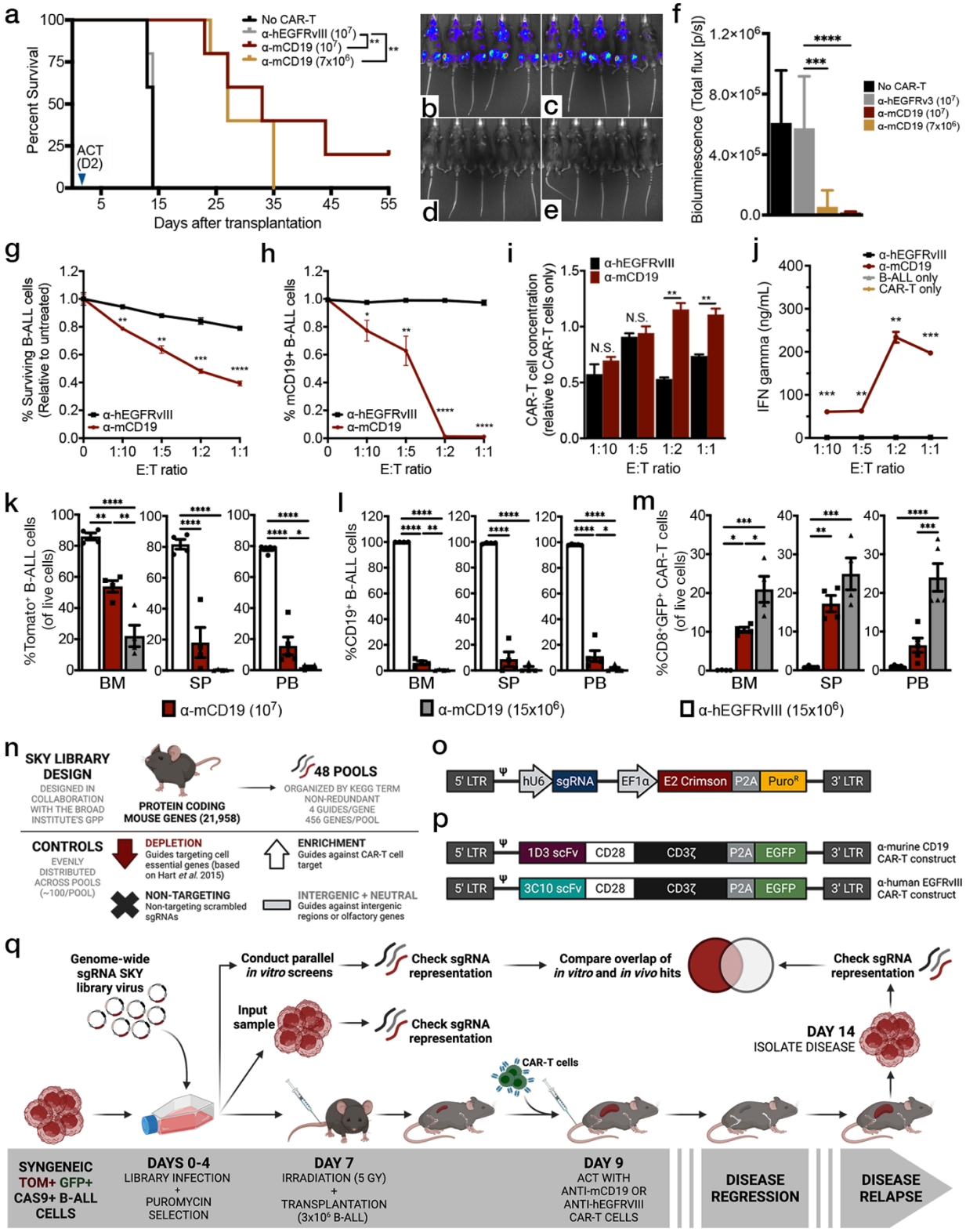
a
Percent Survival
Days after transplantation
ACT (D2)
No CAR-T
α-hEGFRvIII (10^7)
α-mCD19 (10^7)
α-mCD19 (7x10^6)
b
c
d
e
f
Bioluminescence (Total flux [p/s])
No CAR-T
α-hEGFRv3 (10^7)
α-mCD19 (10^7)
α-mCD19 (7x10^6)
g
% Surviving B-ALL cells (Relative to untreated)
E:T ratio
α-hEGFRvIII
α-mCD19
h
% mCD19+ B-ALL cells
i
CAR-T cell concentration (relative to CAR-T cells only)
N.S.
j
IFN gamma (ng/mL)
B-ALL only
CAR-T only
k
%Tomato+ B-ALL cells (of live cells)
BM
SP
PB
α-mCD19 (10^7)
l
%CD19+ B-ALL cells
α-mCD19 (15x10^6)
m
%CD8+GFP+ CAR-T cells (of live cells)
α-hEGFRvIII (15x10^6)
n
SKY LIBRARY DESIGN
DESIGNED IN COLLABORATION WITH THE BROAD INSTITUTE'S GPP
PROTEIN CODING MOUSE GENES (21,958)
48 POOLS
ORGANIZED BY KEGG TERM
NON-REDUNDANT
4 GUIDES/GENE
456 GENES/POOL
CONTROLS
EVENLY DISTRIBUTED ACROSS POOLS (~100/POOL)
DEPLETION
Guides targeting cell essential genes (based on Hart et al. 2015)
ENRICHMENT
Guides against CAR-T cell target
NON-TARGETING
Non-targeting scrambled sgRNAs
INTERGENIC + NEUTRAL
Guides against intergenic regions or olfactory genes
o
5' LTR
Ψ
hU6
sgRNA
EF1α
E2 Crimson
P2A
Puro^R
3' LTR
p
1D3 scFv
CD28
CD3ζ
EGFP
α-murine CD19 CAR-T construct
3C10 scFv
α-human EGFRvIII CAR-T construct
q
Genome-wide sgRNA SKY library virus
Conduct parallel in vitro screens
Check sgRNA representation
Compare overlap of in vitro and in vivo hits
Input sample
CAR-T cells
DAY 14
ISOLATE DISEASE
SYNGENEIC TOM+ GFP+ CAS9+ B-ALL CELLS
DAYS 0-4
LIBRARY INFECTION + PUROMYCIN SELECTION
DAY 7
IRRADIATION (5 GY) + TRANSPLANTATION (3x10^6 B-ALL)
DAY 9
ACT WITH ANTI-mCD19 OR ANTI-hEGFRVIII CAR-T CELLS
DISEASE REGRESSION
DISEASE RELAPSE

768 Figure 2

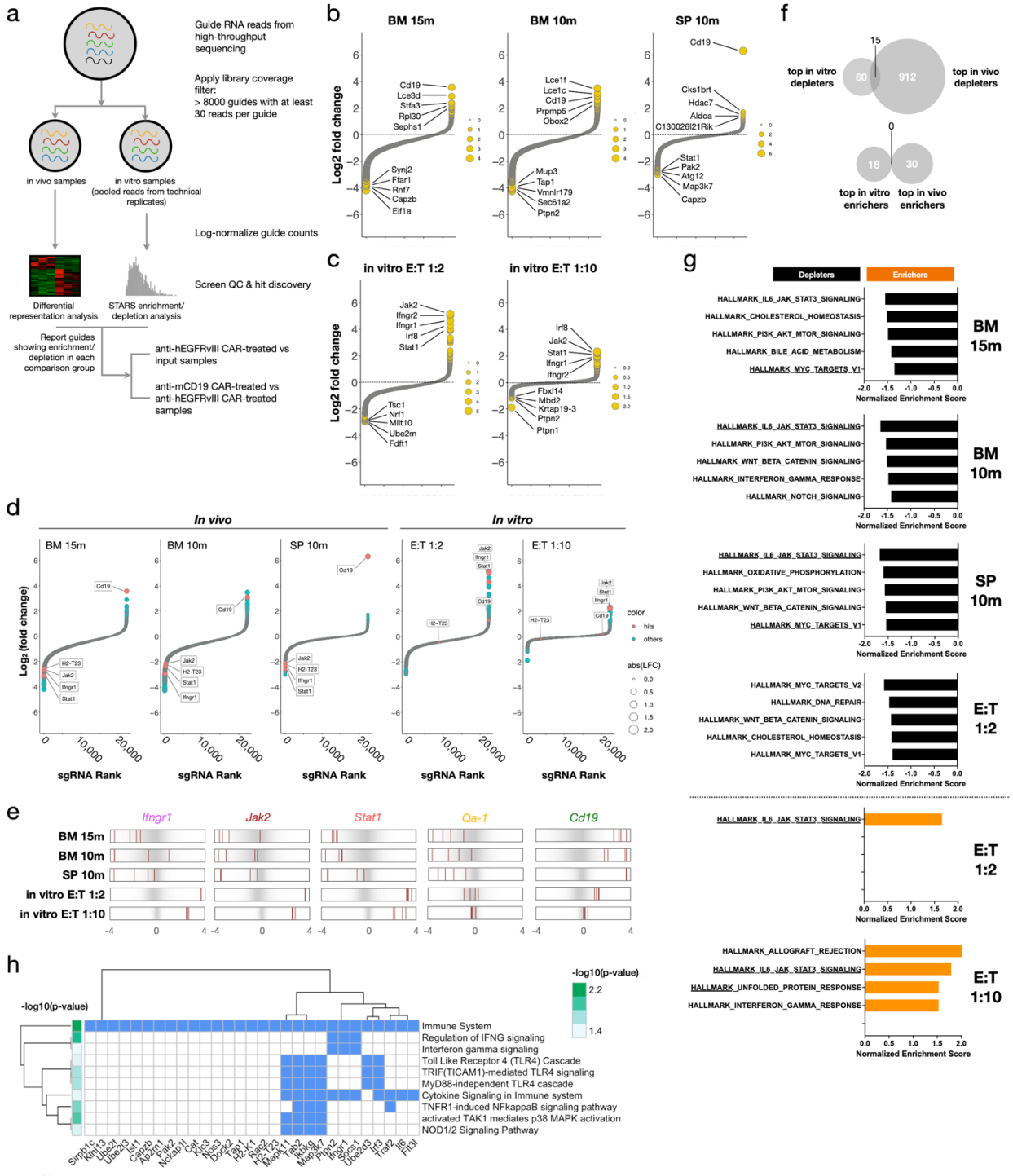
a
Guide RNA reads from high-throughput sequencing
Apply library coverage filter: > 8000 guides with at least 30 reads per guide
in vivo samples
in vitro samples (pooled reads from technical replicates)
Log-normalize guide counts
Differential representation analysis
STARS enrichment/ depletion analysis
Screen QC & hit discovery
Report guides showing enrichment/ depletion in each comparison group
anti-hEGFRvIII CAR-treated vs input samples
anti-mCD19 CAR-treated vs anti-hEGFRvIII CAR-treated samples
b
BM 15m
BM 10m
SP 10m
Log2 fold change
c
in vitro E:T 1:2
in vitro E:T 1:10
d
In vivo
In vitro
BM 15m
BM 10m
SP 10m
E:T 1:2
E:T 1:10
Log2 (fold change)
sgRNA Rank
color
hits
others
abs(LFC)
e
Ifngr1
Jak2
Stat1
Qa-1
Cd19
BM 15m
BM 10m
SP 10m
in vitro E:T 1:2
in vitro E:T 1:10
f
top in vitro depleters
top in vivo depleters
top in vitro enrichers
top in vivo enrichers
g
Depleters
Enrichers
BM 15m
BM 10m
SP 10m
E:T 1:2
E:T 1:10
Normalized Enrichment Score
h
-log10(p-value)
Immune System
Regulation of IFNG signaling
Interferon gamma signaling
Toll Like Receptor 4 (TLR4) Cascade
TRIF(TICAM1)-mediated TLR4 signaling
MyD88-independent TLR4 cascade
Cytokine Signaling in Immune system
TNFR1-induced NFkappaB signaling pathway
activated TAK1 mediates p38 MAPK activation
NOD1/2 Signaling Pathway

770 Figure 3

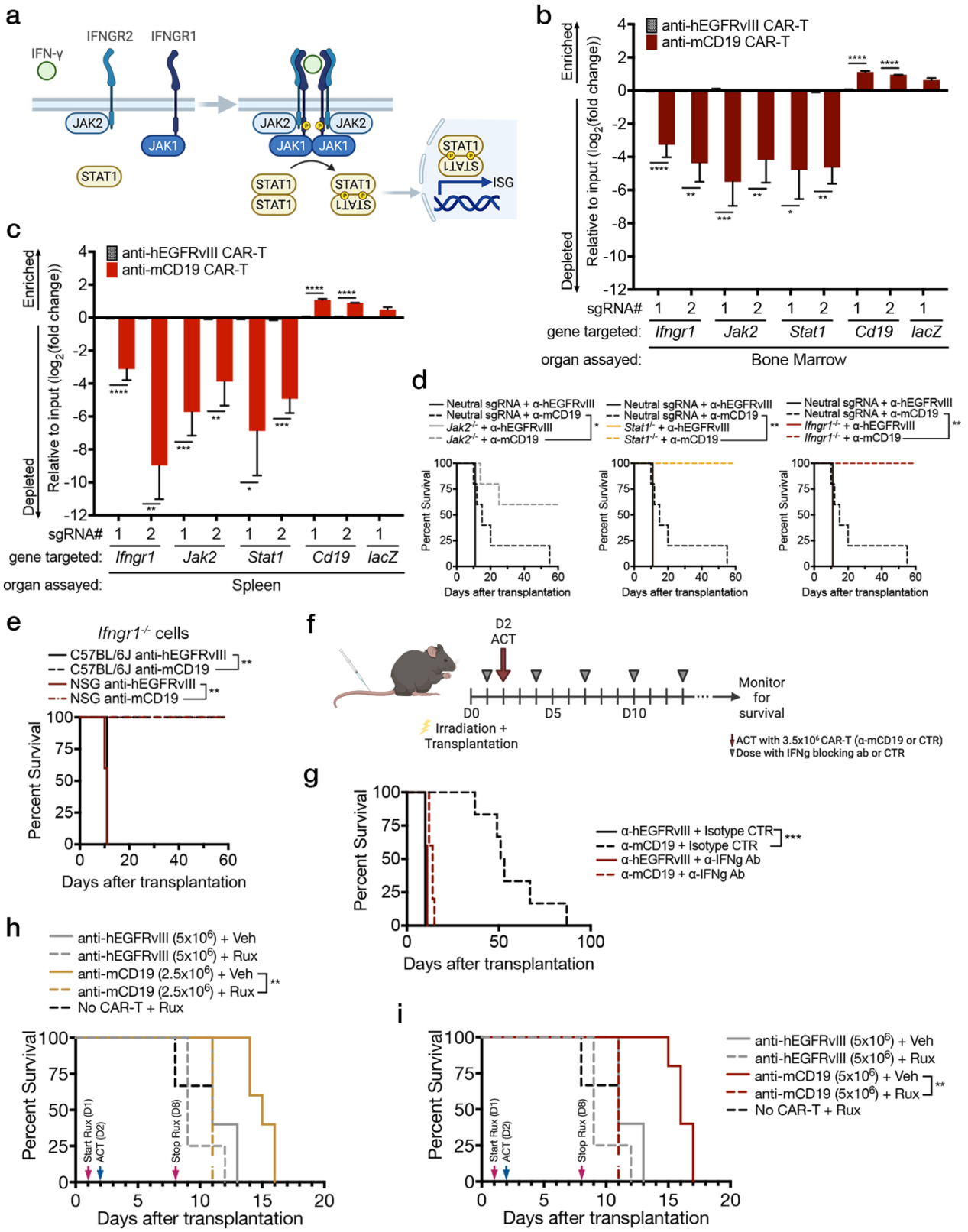
a
IFN-γ
IFNGR2
IFNGR1
JAK2
JAK1
STAT1
ISG
b
anti-hEGFRvIII CAR-T
anti-mCD19 CAR-T
Enriched
Depleted
Relative to input (log2(fold change))
sgRNA#
gene targeted:
Ifngr1
Jak2
Stat1
Cd19
lacZ
organ assayed:
Bone Marrow
c
Spleen
d
Neutral sgRNA + α-hEGFRvIII
Neutral sgRNA + α-mCD19
Jak2-/- + α-hEGFRvIII
Jak2-/- + α-mCD19
Stat1-/- + α-hEGFRvIII
Stat1-/- + α-mCD19
Ifngr1-/- + α-hEGFRvIII
Ifngr1-/- + α-mCD19
Percent Survival
Days after transplantation
e
Ifngr1-/- cells
C57BL/6J anti-hEGFRvIII
C57BL/6J anti-mCD19
NSG anti-hEGFRvIII
NSG anti-mCD19
f
D2
ACT
D0
D5
D10
Monitor for survival
Irradiation + Transplantation
ACT with 3.5x10⁶ CAR-T (α-mCD19 or CTR)
Dose with IFNg blocking ab or CTR
g
α-hEGFRvIII + Isotype CTR
α-mCD19 + Isotype CTR
α-hEGFRvIII + α-IFNg Ab
α-mCD19 + α-IFNg Ab
h
anti-hEGFRvIII (5x10⁶) + Veh
anti-hEGFRvIII (5x10⁶) + Rux
anti-mCD19 (2.5x10⁶) + Veh
anti-mCD19 (2.5x10⁶) + Rux
No CAR-T + Rux
Start Rux (D1)
ACT (D2)
Stop Rux (D8)
i
anti-mCD19 (5x10⁶) + Veh
anti-mCD19 (5x10⁶) + Rux

Figure 4

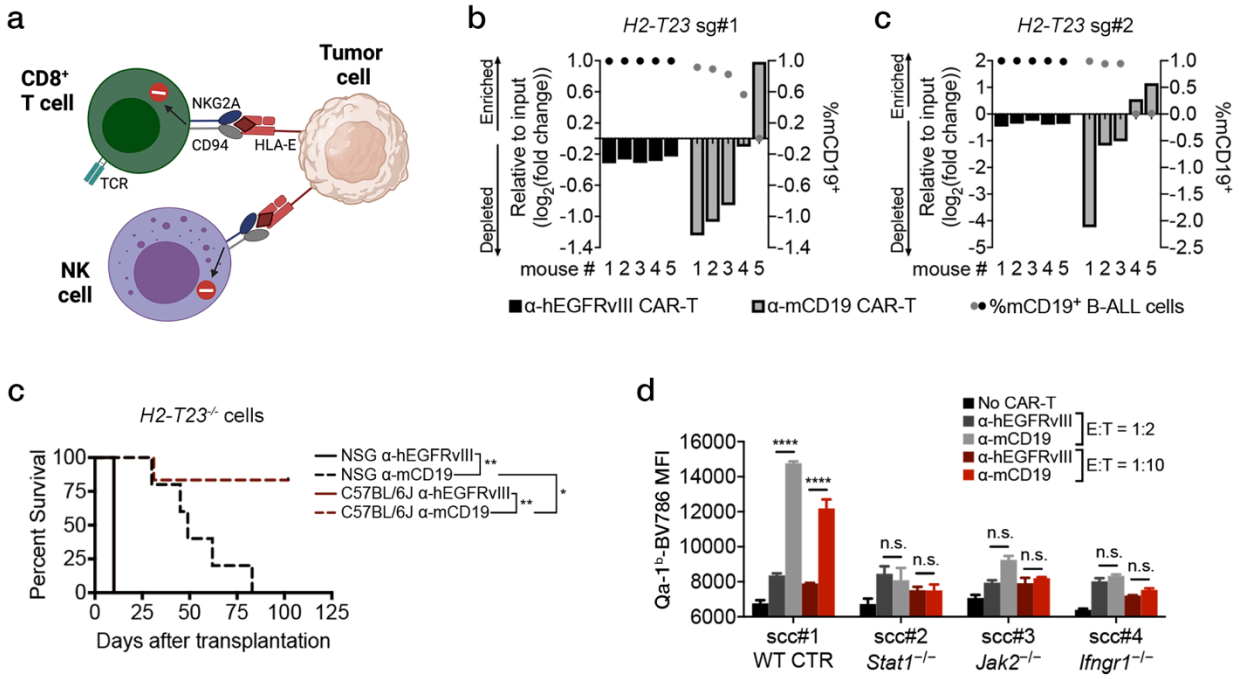
a
CD8+ T cell
Tumor cell
NKG2A
CD94
HLA-E
TCR
NK cell
b
H2-T23 sg#1
Enriched
Depleted
Relative to input (log2(fold change))
%mCD19+
mouse # 1 2 3 4 5 1 2 3 4 5
c
H2-T23 sg#2
α-hEGFRvIII CAR-T
α-mCD19 CAR-T
%mCD19+ B-ALL cells
c
H2-T23-/- cells
Percent Survival
Days after transplantation
NSG α-hEGFRvIII
NSG α-mCD19
C57BL/6J α-hEGFRvIII
C57BL/6J α-mCD19
d
Qa-1b-BV786 MFI
No CAR-T
α-hEGFRvIII
α-mCD19
E:T = 1:2
E:T = 1:10
n.s.
scc#1 WT CTR
scc#2 Stat1-/-
scc#3 Jak2-/-
scc#4 Ifngr1-/-

Figure 5

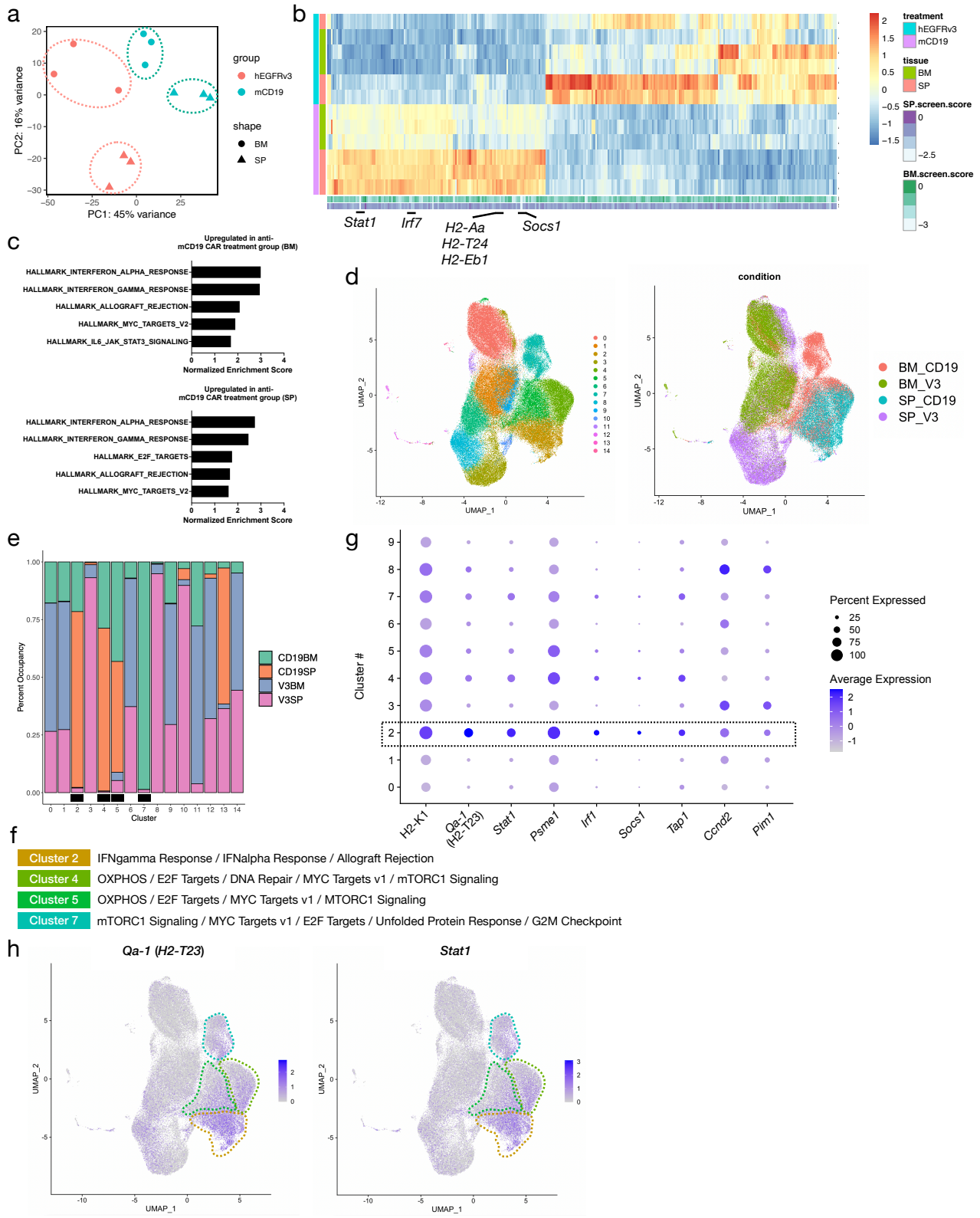
a
PC2: 16% variance
PC1: 45% variance
group
hEGFRv3
mCD19
shape
BM
SP
b
treatment
hEGFRv3
mCD19
tissue
BM
SP
SP.screen.score
BM.screen.score
Stat1
Irf7
H2-Aa
H2-T24
H2-Eb1
Socs1
c
Upregulated in anti-mCD19 CAR treatment group (BM)
HALLMARK_INTERFERON_ALPHA_RESPONSE
HALLMARK_INTERFERON_GAMMA_RESPONSE
HALLMARK_ALLOGRAFT_REJECTION
HALLMARK_MYC_TARGETS_V2
HALLMARK_IL6_JAK_STAT3_SIGNALING
Normalized Enrichment Score
Upregulated in anti-mCD19 CAR treatment group (SP)
HALLMARK_INTERFERON_ALPHA_RESPONSE
HALLMARK_INTERFERON_GAMMA_RESPONSE
HALLMARK_E2F_TARGETS
HALLMARK_ALLOGRAFT_REJECTION
HALLMARK_MYC_TARGETS_V2
Normalized Enrichment Score
d
condition
UMAP_1
UMAP_2
BM_CD19
BM_V3
SP_CD19
SP_V3
e
Percent Occupancy
Cluster
CD19BM
CD19SP
V3BM
V3SP
g
Cluster #
Percent Expressed
Average Expression
H2-K1
Qa-1 (H2-T23)
Stat1
Psme1
Irf1
Socs1
Tap1
Ccnd2
Pim1
f
Cluster 2 IFNgamma Response / IFNalpha Response / Allograft Rejection
Cluster 4 OXPHOS / E2F Targets / DNA Repair / MYC Targets v1 / mTORC1 Signaling
Cluster 5 OXPHOS / E2F Targets / MYC Targets v1 / MTORC1 Signaling
Cluster 7 mTORC1 Signaling / MYC Targets v1 / E2F Targets / Unfolded Protein Response / G2M Checkpoint
h
Qa-1 (H2-T23)
Stat1
UMAP_1
UMAP_2

794

Figure 6

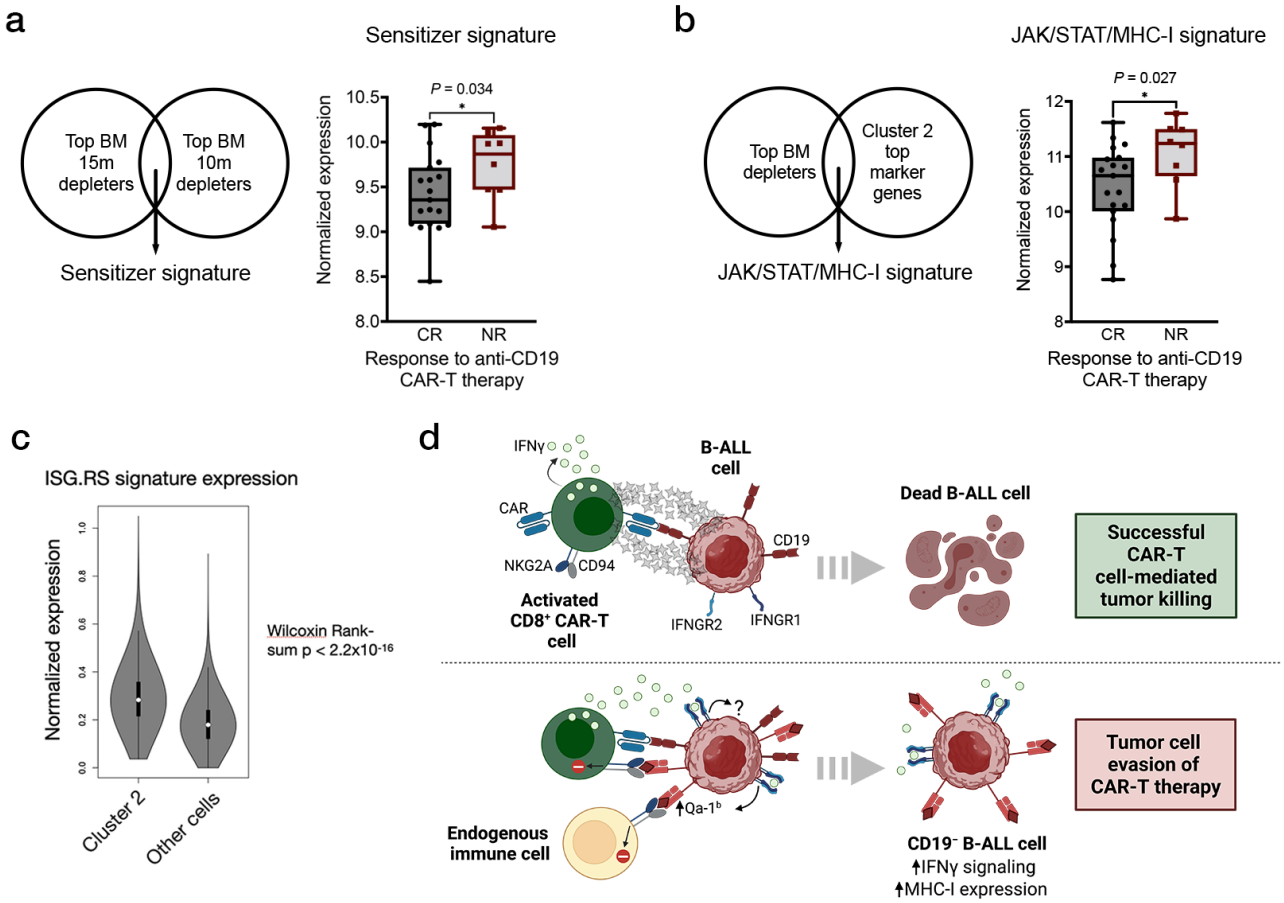
a
Sensitizer signature
Top BM 15m depleters
Top BM 10m depleters
Sensitizer signature
P = 0.034
Normalized expression
CR
NR
Response to anti-CD19 CAR-T therapy
b
JAK/STAT/MHC-I signature
Top BM depleters
Cluster 2 top marker genes
JAK/STAT/MHC-I signature
P = 0.027
Normalized expression
CR
NR
Response to anti-CD19 CAR-T therapy
c
ISG.RS signature expression
Normalized expression
Wilcoxin Rank-sum p < 2.2x10-16
Cluster 2
Other cells
d
IFNγ
B-ALL cell
CAR
NKG2A
CD94
CD19
Activated CD8+ CAR-T cell
IFNGR2
IFNGR1
Dead B-ALL cell
Successful CAR-T cell-mediated tumor killing
Qa-1b
Endogenous immune cell
CD19− B-ALL cell
↑IFNγ signaling
↑MHC-I expression
Tumor cell evasion of CAR-T therapy

Supplementary Figure 1

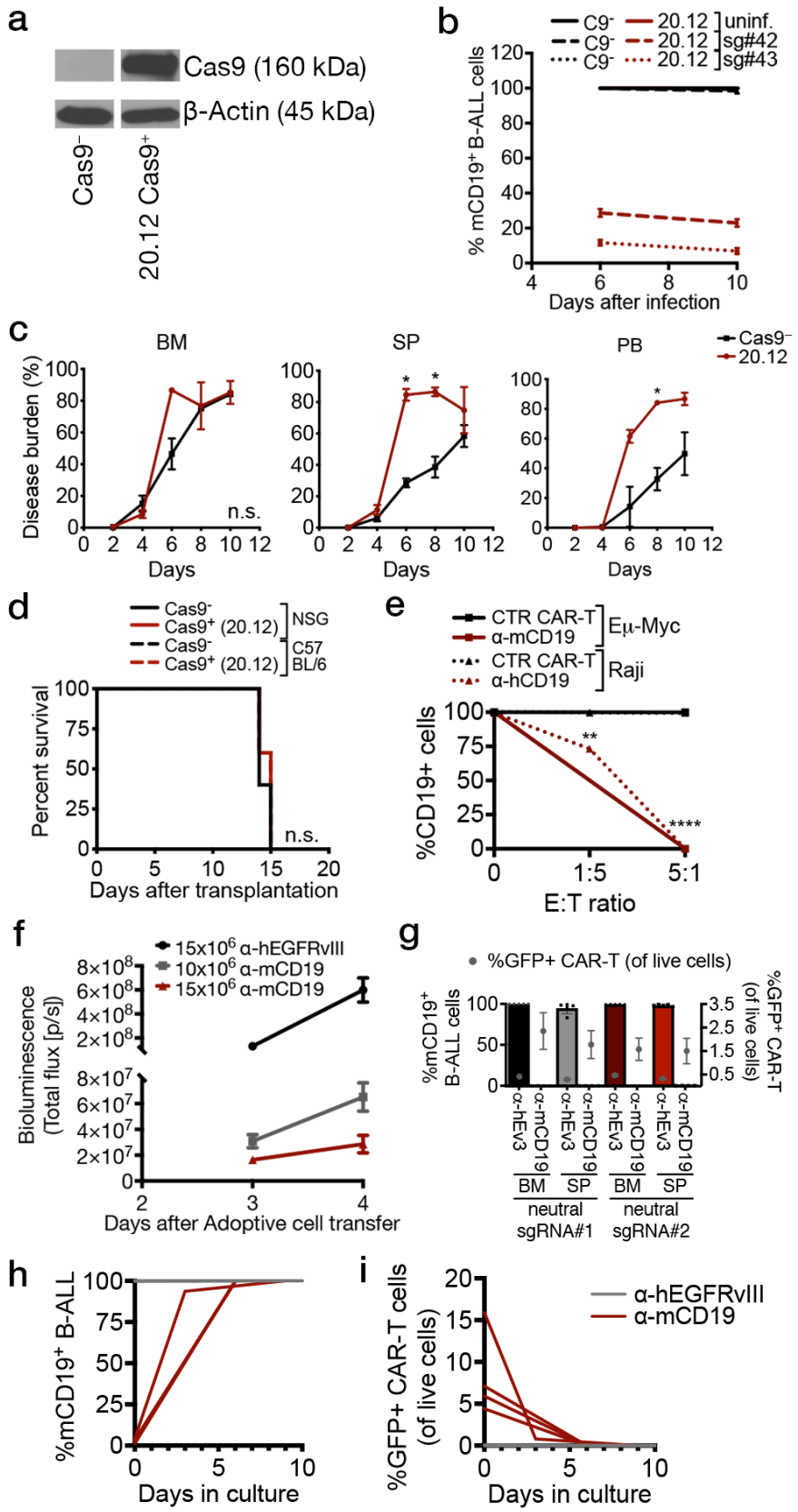

814

Supplementary Figure 2

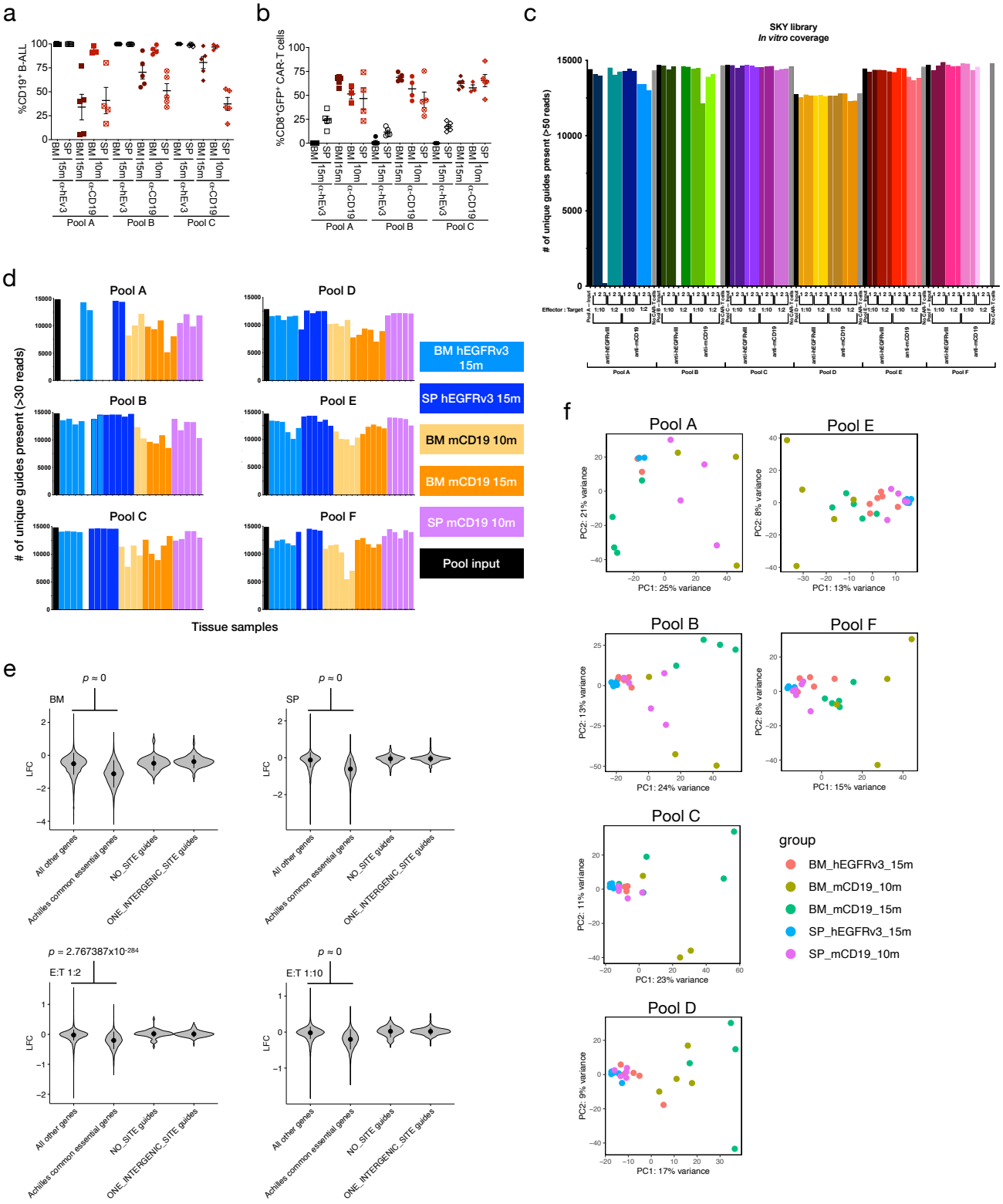

816

Supplementary Figure 3

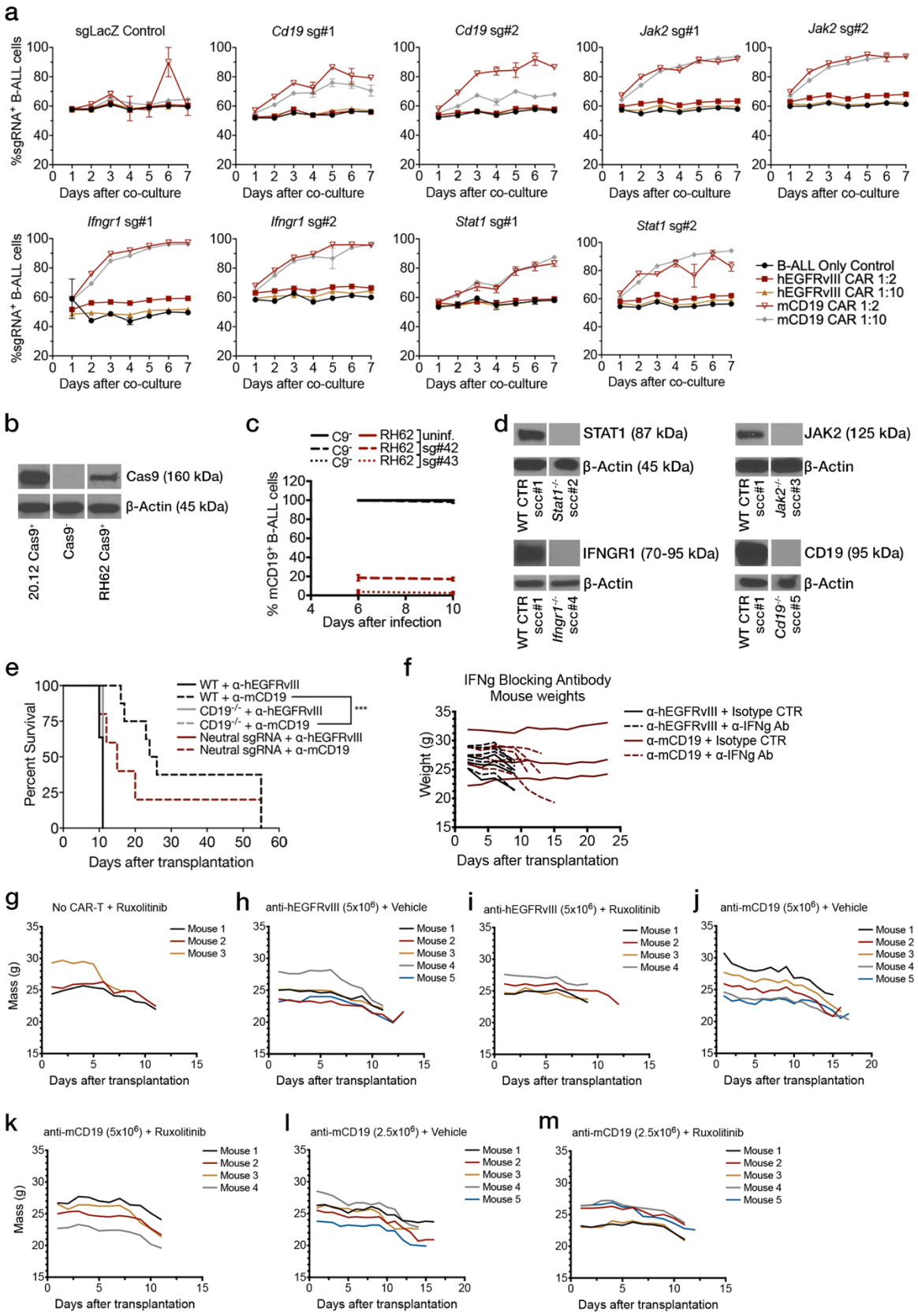

818

Supplementary Figure 4

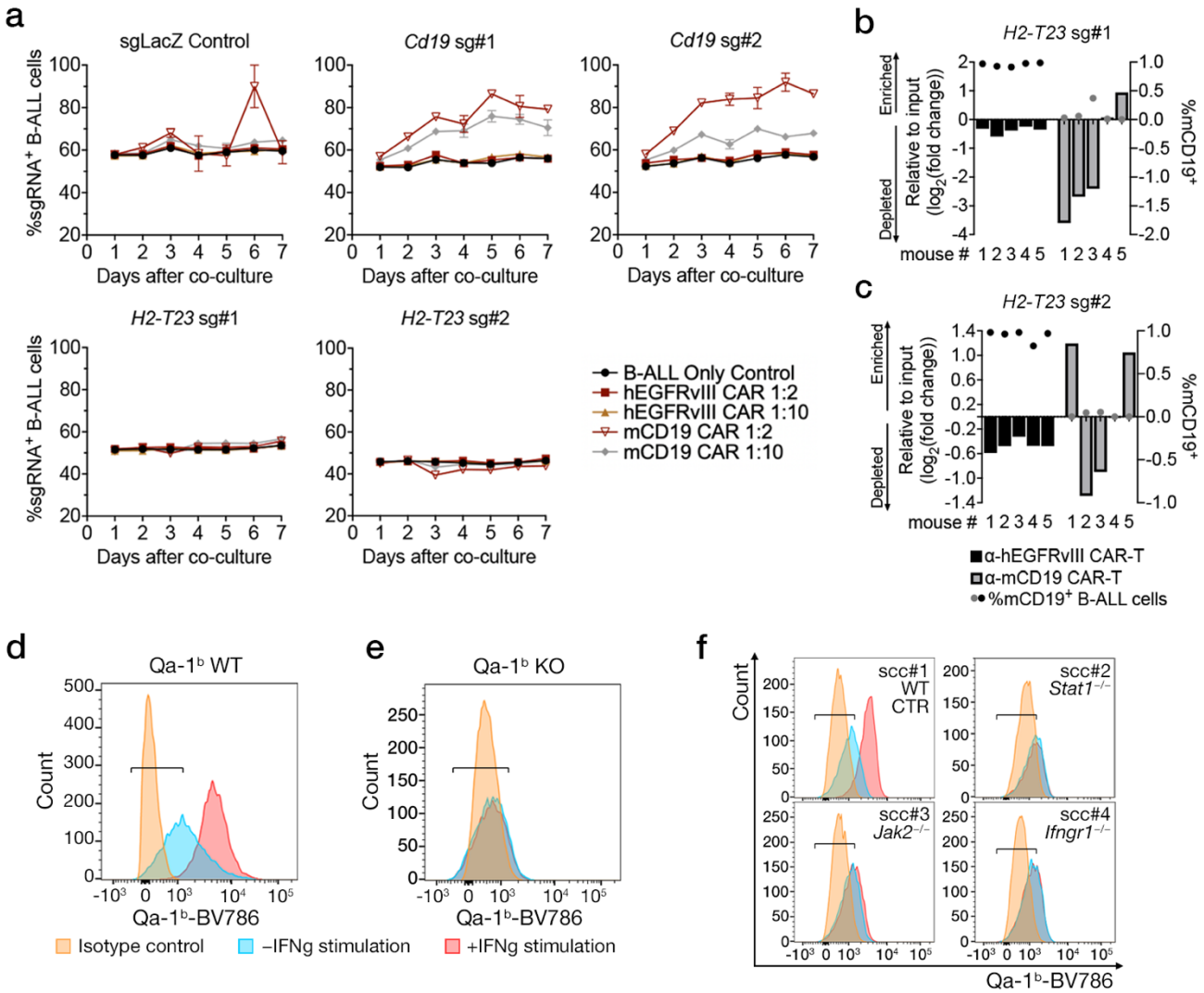

Supplementary Figure 5

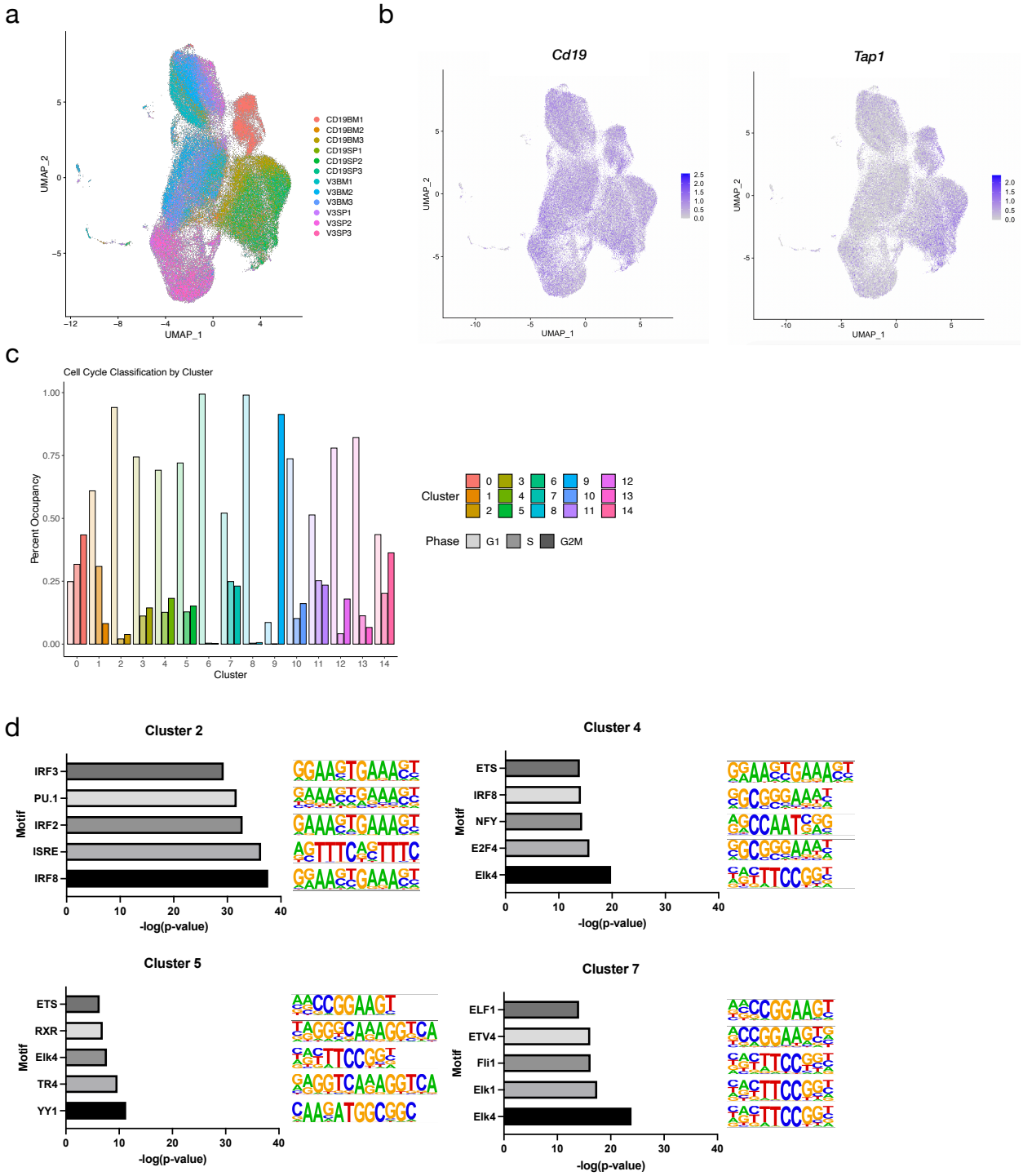

Figure Legends

840 **Figure 1. A fully immunocompetent mouse model of BCR-ABL1$^+$ B-ALL enables parallel *in vivo* and *in vitro* genome-wide screens for CAR-T resistance.** (a) Survival curves and analysis
842 of irradiated B6 mice inoculated with syngeneic B-ALL cells and treated with indicated CAR-T cell type. Mice treated with CAR-T cells targeting murine CD19 (mCD19) showed significant life
844 extension in a dose-dependent manner, as compared to those treated with no CAR-T cells or control CAR-T cells against human EGFRvIII (hEGFRvIII or hEGFRv3). Bioluminescence imaging
846 four days after adoptive cell transfer (ACT) showed significant disease burden in (b) mice not treated with CAR-T cells and (c) mice treated with control CAR-T cells. Conversely, mice treated
848 with mCD19 CAR-T cells at a dose of either (d) $7x10^6$ or (e) 10^7 show (f) significant disease suppression. (g) *In vitro* cytotoxicity assays show significant depletion of tumor cells along with
850 (h) massive target epitope loss when B-ALL cells are treated with anti-mCD19 CAR-T cells at increasing effector to target cell (E:T) ratios. (i) Concomitantly, CAR-T cells expand and (j) release
852 IFN**γ** when co-cultured with mCD19+ B-ALL cells. (k-m) Experiments to determine the appropriate dose of CAR-T cells for either the marrow (BM) or spleen (SP). Peripheral blood (PB) was also
854 assessed. Mice sacrificed four days after ACT showed an 80% reduction in marrow disease at a dose of $1.5x10^7$ anti-mCD19 CAR-T cells, while identical disease suppression in the spleen and
856 blood was accomplished with 10^7 CAR-T cells. (l) Massive target epitope loss and (m) significant CAR-T cell persistence was also observed in all of the organs harvested from mice treated with
858 anti-mCD19 CAR-T cells. (n) Schematic showing the overall design and (o) lentiviral backbone used to create the SKY library. (p) Retroviral vectors encoding the 1D3 single chain variable
860 fragment (scFv) targeting mCD19 (top) and the 3C10 scFv targeting hEGFRvIII (bottom). (q) Diagram of screening layout. Significance for survival experiments was determined using log-rank
862 tests. For all other experiments, significance is determined using unpaired two-sided student's t-tests with Bonferroni correction for multiple comparisons, or using one-way ANOVA with Turkey's
864 correction for multiple comparisons when more than two groups were compared. Data are mean ± s.e.m.; n = 4–6 mice per group). *P<0.05; **P < 0.01; ***P < 0.001; ****P < 0.001.

866

Figure 2. *In vivo* genome-wide CRISPR-Cas9-mediated knockout screen identifies Jak/Stat
868 **and antigen presentation pathways involved in resistance to CAR-T therapy.** (a) Schematic of the data analysis and screen hit discovery workflow. (b-c) Waterfall plots of log-fold changes of
870 the representation of gRNA against different genes in anti-mCD19 CAR-T cell treated animals (b) or cells (c) compared to anti-hEGFRvIII CAR-T cell treated (control) animals (b) or cells (c). Genes
872 are ranked by the average log-fold changes of all gRNAs against each gene, and point sizes are

proportional to the magnitude (absolute value) of log-fold changes. Top 5 genes with
874 enriching/depleting gRNAs are labeled. (d) Waterfall plots of the relative significance of each hit (vertical axis, showing log2(fold change) from two-sided student's t-test with correction for multiple
876 comparisons or STARS analysis) versus guide ranks. (e) Relative enrichment/depletion of individual guides against top depleters *Ifngr1*, *Jak2*, *Stat1,* and *Qa-1* are shown in each arm of
878 the screen. Guide RNAs against *Cd19* are also shown as an indicator of CAR-T treatment pressure. (f) Venn diagrams showing overlap of top hits from the *in vitro* and *in vivo* arms of the
880 screen. Top hits are defined as genes with an absolute log-fold change greater than 2. (g) Bar plots of GSEA analysis of top depleting (black) or enriching (orange) hits in each arm of the
882 screen. Plots show up to the top 5 Hallmark pathways with enrichment FDR value smaller than 0.05 enriched Hallmark pathways. (h) Enrichment of KEGG terms within genes showing top gRNA
884 depletion in the *in vivo* arms of the screen. Shown is a heatmap of participation of the top genes in each enriched pathway.

886

Figure 3. Loss of components of the IFNγ/JAK/STAT pathway sensitizes tumors to CAR-T
888 **therapy *in vivo*.** (a) Schematic showing the IFN**γ** signaling pathway. (b-c) *In vivo* competitive assays demonstrate specific log-fold depletion of Cas9$^+$ RH62 B-ALL cells lacking components
890 of the IFN**γ**/JAK/STAT pathway and enrichment of B-ALL cells lacking mCD19 after treatment with anti-mCD19 CAR-T cells in both (b) the bone marrow and (c) the spleen. (d)
892 Immunocompetent (B6) and (e) immunocompromised (NSG) mice transplanted with B-ALL cells deficient in indicated components of the IFN**γ**/JAK/STAT pathway survive significantly longer than
894 control mice. (f) Layout and treatment schedule for anti-IFN**γ** blocking antibody experiment. (g) Blocking IFN**γ** signaling concurrently with CAR-T therapy eliminates the antitumor capabilities of
896 CAR-T cells. Concurrent treatment of Ruxolitinib, a JAK1/2 inhibitor, with either $2.5x10^6$ (h) or $5x10^6$ (i) CAR-T cells also eliminates any benefit of CAR-T therapy. Significance for survival
898 experiments was determined using log-rank tests. For all other experiments, significance is determined using unpaired two-sided student's t-tests with Bonferroni correction for multiple
900 comparisons. Data are mean ± s.e.m.; n = 5-8 mice per group). *P<0.05; **P < 0.01; ***P < 0.001; ****P < 0.001.

902

Figure 4. Loss of Qa-1^b, a component of the MHC-I pathway, sensitizes B-ALL cells to CAR-
904 **T therapy *in vivo*.** (a) Schematic showing the known effect of the HLA-E/NKG2A/CD94 axis in NK and CD8$^+$ T cells. (b, c) *In vivo* competitive assays using two independent guides against the
906 non-classical MHC-I gene *H2-T23*. Tumors harvested from the bone marrow of relapsed mice

demonstrate significant depletion of *H2-T23* null populations after treatment with anti-mCD19
908 CAR-T cells only when *H2-T23* null cells also relapse mCD19^{+}. (c) Immunocompetent (B6) mice transplanted with Qa-1^{b}-deficient B-ALL cells show increased survival as compared to
910 immunocompromised (NSG) after treatment with anti-mCD19 CAR-T cells. (d) Mean fluorescence intensity (MFI) of Qa-1^{b}-Brilliant Violet 786 (BV786) after *in vitro* CAR-T treatment of single cell
912 clones (scc) deficient in indicated components of the IFN**γ**/JAK/STAT pathway at two different E:T ratios, as assayed using flow cytometry. Wildtype control single cell clones were also
914 generated and assayed at the same time. Representative data for WT control clones is shown in (d). Significance for survival experiments was determined using log-rank tests. For all other
916 experiments, significance is determined using unpaired two-sided student's t-tests with Bonferroni correction for multiple comparisons. Data are mean ± s.e.m.; n = 5-8 mice per group). *P<0.05;
918 **P < 0.01; ***P < 0.001; ****P < 0.001.

920 **Figure 5. Bulk and single cell gene expression profiling pinpoints specific cell subsets and expression programs as a source of CAR-T cell resistance in B-ALL.** (a) PCA plot of bulk
922 RNA-seq profiles of bone marrow (BM) and spleen (SP) samples collected from mice treated with either anti-mCD19 or anti-hEGFRvIII (control) CAR T cells. (b) Heatmap of genes differentially
924 expressed between anti-mCD19 and anti-hEGFRvIII CAR T cell-treated samples. Scores of genes from the screen are shown next to each gene's expression profile (column). Top depleters
926 in the bone marrow and spleen samples are labeled. (c) Top Hallmark gene sets enriched among genes overexpressed in mCD19 CAR T cell therapy compared to control treated bone marrow
928 (BM) or spleen (SP) samples. Bar graphs show normalized enrichment scores for each of the top 5 enriched pathways. Enrichment analysis was performed using GSEA and all pathways shown
930 have FDR < 0.05. (d) 2-dimensional UMAP plots of single cell gene expression profiles collected from mice treated with either anti-mCD19 or anti-hEGFRvIII CAR T cell therapy. Data are
932 collected from n=3 mice per treatment group. Left panel: cells color-coded by clusters discovered through unsupervised clustering; right panel: cells color-coded by treatment and tissue groups.
934 (e) Participation of cells from each tissue/treatment group in each cluster. Bar graphs show percentage of cells in each cluster belonging to each tissue/treatment group. Clusters where there
936 is substantial enrichment of cells under anti-mCD19 CAR T therapy are marked with a black box underneath the bar plots. (f) Hallmark gene sets enriched in the 4 treatment-specific clusters as
938 labeled in (e). (g) Dot plot showing relative expression patterns of cluster 2 marker genes which are also among top depleters (log2 fold change < -1.75) in the BM samples of the *in vivo* screen.
940 Dot size is proportional to the percentage of cells in each cluster expressing each gene and dot

color indicates average expression of each gene in each cluster. (h) UMAP plots showing
942 expression of *Qa-1* and *Stat1* in single cell samples, with cells color-coded by expression levels.

944 **Figure 6. JAK/STAT signaling is a potential therapeutic target in human B-ALL that can be exploited to enhance CAR-T therapy.** (a) A gene signature composed of top depleters in
946 the bone marrow is expressed at a lower level in complete responders (CR) to CAR-T therapy and is thus associated with better outcomes in B-ALL patients. Non-responders (NR) show
948 increased expression of these genes, indicating an association with CAR-T resistance. (b) Higher expression of a JAK/STAT/MHC-I resistance signature is associated with poor outcomes
950 in CAR-T treated patients. (c) After CAR-T failure, relapsed B-ALL cells exhibit increased expression of ICB resistance-associated interferon stimulated genes (ISG.RS) that is also
952 associated with poor outcomes in CAR-T treated large B cell lymphoma patients. (d) A final model for how high JAK/STAT/IFN**γ** signaling in tumor cells can promote resistance to CAR-T
954 therapy. Significance is determined using unpaired two-sided student's t-tests with Bonferroni correction for multiple comparisons. Data are mean ± s.e.m.). *P<0.05; **P < 0.01; ***P < 0.001;
956 ****P < 0.001.

958 **Supplementary Figure 1. Characterization of Cas9+ disease and target epitope loss after CAR-T treatment.** (a) Cas9 expression in 20.12 cells assayed via western blot. (b) *In vitro* cut
960 assay using two validated, non-overlapping guides against murine CD19 (mCD19) was used to determine Cas9 cutting efficiency in 20.12 cells. Eight days after the introduction of sgRNAs, more
962 than 75% of all 20.12 cells are mCD19^{-}. (c) Tomato^{+} GFP^{+} Cas9^{+} 20.12 cells show similar or faster growth kinetics as non-Cas9 expressing parental cells in hematopoietic organs of non-irradiated
964 syngeneic B6 mice, as assayed by flow cytometry. (d) Non-irradiated immunocompetent (B6) mice and immunocompromised (NSG) mice succumbed to both Cas9^{-} and Cas9^{+} (20.12) disease
966 at the same time, indicating that Cas9 is not additionally immunogenic *in vivo.* (e) Murine CAR-T cells targeting either mCD19 or human CD19 (FMC63 scFv) *in vitro* induce dose dependent target
968 epitope loss in murine Eμ-Myc and human Raji cells, respectively. (f) Bioluminescence imaging of irradiated B6 mice treated with indicated CAR-T cell type and dose at indicated time after ACT.
970 (g) Organs from moribund control mice that relapsed after treatment with 3.5 x10^{6} CAR-T cells targeting mCD19 demonstrate ongoing CAR-T engraftment and complete target epitope loss in
972 B-ALL cells. (h) Whole spleens relapsed mice after treatment with 5x10^{6} indicated CAR-T cell type were dissociated, cultured *in vitro* and serially assessed for mCD19^{+} B-ALL and GFP^{+} CAR-
974 T cells. As anti-mCD19 CAR-T cells are depleted out of culture, B-ALL cells re-express mCD19.

Significance for survival experiments was determined using log-rank tests. For all other
976 experiments, significance is determined using unpaired two-sided student's t-tests with Bonferroni correction for multiple comparisons. Data are mean ± s.e.m.; n = 4–8 mice per group. *P<0.05;
978 **P < 0.01; ***P < 0.001; ****P < 0.001.

980 **Supplemental Figure 2. *In vitro* and *in vivo* genome-wide CRISPR/Cas9-mediated screens show comprehensive representation of sgRNA libraries and capture differences in sgRNA**
982 **behavior in between control and anti-mCD19 CAR-T treated mice.** (a) Flow cytometry assay investigating the proportion of CD19+ B-ALL cells in the spleen (SP) or bone marrow (BM) after
984 treatment with the indicated CAR-T cell type (anti-CD19 versus control anti-human EGFRvIII) and dose. (b) Flow cytometry assay investigating the proportion of persistent CAR-T cells in the spleen
986 (SP) or bone marrow (BM) after treatment with the indicated CAR-T cell type. Data are mean ± s.e.m.; n = 3–5 mice per group. (c) sgRNA library representation in each pooled library in
988 the *in vitro* screen samples. Each bar shows the number of sgRNAs with more than 30 reads in the sequencing sample for a given pool. (d) Same as (c), but for sgRNA library representation in
990 each pooled library in the *in vivo* screen samples. (e) Violin plots showing relative depletion/enrichment of control sgRNAs used in the screen. *P*-values are calculated from Wilcoxin
992 rank-sum tests for comparison between pairs of group means. Note that in some cases exact *p*-values cannot be determined due to extremely near-zero values and ties in data and are reported
994 as approximately zero. (f) *In vivo* screen samples projected onto the first 2 principal components of input-normalized sgRNA count matrix.

996

Supplemental Figure 3. *In vitro* cytotoxicity assays in cells deficient for components of the
998 **IFNγ/JAK/STAT pathway do not capture *in vivo* sensitization phenotypes to CAR-T therapy.** (a) *In vitro* competitive assays completed in cells transduced with guides against the indicated
1000 IFNγ/JAK/STAT pathway or control gene and treated with the indicated CAR-T cell type at two E:T ratios. (b) Western blot showing that Tomato+ RH62 B-ALL cells used for all validation
1002 experiments express Cas9 protein. (c) *In vitro* cut assay using two validated, non-overlapping guides against murine CD19 (mCD19) was used to determine Cas9 cutting efficiency in RH62
1004 cells. Six days after the introduction of sgRNAs, more than 75% of all RH62 cells are mCD19^{-}. (d) Western blot analysis of single cell clones (scc) deficient in indicated gene and used in survival
1006 validation experiments. (e) Mice transplanted with parental (WT) or neutral control cells do not significantly differ in their survival after treatment with anti-mCD19 CAR-T cells, while mice
1008 transplanted with *Cd19*$^{-/-}$ B-ALL cells show no life extension. (f) Mouse weight monitoring over

time during co-treatment with CAR-T cells and anti-IFN**γ** blocking antibodies shows no additional
1010 toxicity during combination therapy. (g-m) Mouse weight monitoring over time during co-treatment with CAR-T cells and Ruxolitinib shows no additional toxicity during combination therapy. Data
1012 are exact mass in grams over time; n = 3-5 mice per group. Significance for survival experiments was determined using log-rank tests. Data are mean ± s.e.m.; n = 5-8 mice per group. *P<0.05;
1014 **P < 0.01; ***P < 0.001; ****P < 0.001.

1016 **Supplementary Figure 4. Loss of Qa-1^b does not sensitize B-ALL cells to CAR-T therapy *in vitro*.**
1018 a) *In vitro* competitive assays completed in cells transduced with single guide RNAs (sg) against *H2-T23* or the indicated control gene and treated with the indicated CAR-T cell type at two E:T
1020 ratios. (b-c) *In vivo* competitive assays using two independent guides against the non-classical MHC-I gene *H2-T23.* All mice relapsed with mCD19$^-$ splenic disease. (d-e) FACS histograms
1022 showing Qa-1^b expression on cells transduced with a control sgRNA (Qa-1^b WT) or Qa-1^b-deficient cells after stimulation with IFN**γ**. Black brackets indicate gating for Qa-1^b-negative cell
1024 populations (gating is set to strictly exclude Qa-1^b-positive populations, to ensure pure populations were isolated upon cell sorting). (f) Expression of Qa-1^b-BV786 after *in vitro* stimulation with IFN**γ**
1026 of single cell clones (scc) deficient in indicated components of the IFN**γ**/JAK/STAT pathway, as assayed using flow cytometry. Wildtype control single cell clones were also generated and
1028 assayed at the same time. Representative data for WT control clones is also shown in (f). For all flow cytometry experiments, data for a minimum of 10,000 live cells were collected and analyzed.
1030 Data are mean ± s.e.m.; n = 5 mice per group.

1032 **Supplemental Figure 5. Additional characterizations of clusters that emerge from single-cell expression profiling of CAR-T cell treated animals.** (a) 2-dimensional UMAP plots of
1034 single cell gene expression profiles collected from mice treated with either anti-mCD19 or anti-hEGFRvIII CAR T cell therapy, with cells color-coded by each individual mouse in the dataset. (b)
1036 UMAP plot showing expression of *Cd19* (left panel) and *Tap1* (right panel) in the single cell expression dataset. (c) Proportions of cells assigned to each cell cycle stage in each of the 15
1038 clusters identified in the single cell expression data. (d) Transcription factor motif enrichment analysis for signature genes in clusters 2, 4, 5 and 7. Shown are -log10 transformed *p*-values for
1040 top 5 enriched motifs along with their position-weight matrix logos for each cluster.

1042

1044 **References**

1046 1. Tang, J., Shalabi, A. & Hubbard-Lucey, V. M. Comprehensive analysis of the clinical immuno-oncology landscape. *Ann. Oncol.* **29**, 84–91 (2018).
1048 2. June, C. H. & Sadelain, M. Chimeric antigen receptor therapy. *N. Engl. J. Med.* **379**, 64–73 (2018).
1050 3. June, C. H., O'Connor, R. S., Kawalekar, O. U., Ghassemi, S. & Milone, M. C. CAR T cell immunotherapy for human cancer. *Science (80-.).* **359**, 1361–1365 (2018).
1052 4. Locke, F. L. *et al.* Phase 1 Results of ZUMA-1: A Multicenter Study of KTE-C19 Anti-CD19 CAR T Cell Therapy in Refractory Aggressive Lymphoma. *Mol. Ther.* **25**, 285–295
1054 (2017).
5. Maude, S. L. *et al.* Tisagenlecleucel in children and young adults with B-cell
1056 lymphoblastic leukemia. *N. Engl. J. Med.* **378**, 439–448 (2018).
6. Schuster, S. J. *et al.* Chimeric antigen receptor T Cells in refractory B-Cell lymphomas. *N.*
1058 *Engl. J. Med.* **377**, 2545–2554 (2017).
7. Lee, D. W. *et al.* T cells expressing CD19 chimeric antigen receptors for acute
1060 lymphoblastic leukaemia in children and young adults: A phase 1 dose-escalation trial. *Lancet* **385**, 517–528 (2015).
1062 8. Park, J. H. *et al.* Long-Term Follow-up of CD19 CAR Therapy in Acute Lymphoblastic Leukemia. *N. Engl. J. Med.* **378**, 449–459 (2018).
1064 9. Fry, T. J. *et al.* CD22-targeted CAR T cells induce remission in B-ALL that is naive or resistant to CD19-targeted CAR immunotherapy. *Nat. Med.* **24**, 20–28 (2018).
1066 10. Hay, K. A. *et al.* Factors associated with durable EFS in adult B-cell ALL patients achieving MRD-negative CR after CD19 CAR T-cell therapy. *Blood* **133**, 1652–1663
1068 (2019).
11. Schuster, S. J. *et al.* Tisagenlecleucel in adult relapsed or refractory diffuse large B-cell
1070 lymphoma. *N. Engl. J. Med.* **380**, 45–56 (2019).
12. Neelapu, S. S. *et al.* Axicabtagene ciloleucel CAR T-cell therapy in refractory large B-Cell
1072 lymphoma. *N. Engl. J. Med.* **377**, 2531–2544 (2017).
13. Wang, M. *et al.* KTE-X19 CAR T-Cell Therapy in Relapsed or Refractory Mantle-Cell
1074 Lymphoma. *N. Engl. J. Med.* **382**, 1331–1342 (2020).
14. Fraietta, J. A. *et al.* Determinants of response and resistance to CD19 chimeric antigen
1076 receptor (CAR) T cell therapy of chronic lymphocytic leukemia. *Nat. Med.* **24**, 563–571 (2018).
1078 15. Larson, R. C. & Maus, M. V. Recent advances and discoveries in the mechanisms and functions of CAR T cells. *Nat. Rev. Cancer* **21**, 145–161 (2021).
1080 16. Finney, O. C. *et al.* CD19 CAR T cell product and disease attributes predict leukemia remission durability. *J. Clin. Invest.* **129**, 2123–2132 (2019).
1082 17. Fraietta, J. A. *et al.* Determinants of response and resistance to CD19 chimeric antigen receptor (CAR) T cell therapy of chronic lymphocytic leukemia. *Nat. Med.* **24**, 563–571
1084 (2018).
18. Orlando, E. J. *et al.* Genetic mechanisms of target antigen loss in CAR19 therapy of
1086 acute lymphoblastic leukemia. *Nat. Med.* **24**, 1504–1506 (2018).
19. Grupp, S. A. *et al.* Chimeric Antigen Receptor–Modified T Cells for Acute Lymphoid
1088 Leukemia. *N. Engl. J. Med.* **368**, 1509–1518 (2013).
20. Majzner, R. G. & Mackall, C. L. Tumor antigen escape from car t-cell therapy. *Cancer*
1090 *Discov.* **8**, 1219–26 (2018).
21. Xu, X. *et al.* Mechanisms of Relapse After CD19 CAR T-Cell Therapy for Acute
1092 Lymphoblastic Leukemia and Its Prevention and Treatment Strategies. *Front. Immunol.* **10**, 1–15 (2019).
1094 22. Singh, N. *et al.* Impaired Death Receptor Signaling in Leukemia Causes Antigen-

Independent Resistance by Inducing CAR T-cell Dysfunction. *Cancer Discov.* **10**, 552–567 (2020).

23. Williams, R. T., Roussel, M. F. & Sherr, C. J. Arf gene loss enhances oncogenicity and limits imatinib response in mouse models of Bcr-Abl-induced acute lymphoblastic leukemia. *Proc. Natl. Acad. Sci. U. S. A.* **103**, 6688–6693 (2006).
24. Williams, R. T., Besten, W. Den & Sherr, C. J. Cytokine-dependent imatinib resistance in mouse. *Genes Dev.* **21**, 2283–2287 (2007).
25. Meacham, C. E. *et al.* A genome-scale in vivo loss-of-function screen identifies phf6 as a lineage-specific regulator of leukemia cell growth. *Genes Dev.* **29**, 483–488 (2015).
26. Fiedler, E. R. C., Bhutkar, A., Lawler, E., Besada, R. & Hemann, M. T. In vivo RNAi screening identifies Pafah1b3 as a target for combination therapy with TKIs in BCR-ABL11 BCP-ALL. *Blood Adv.* **2**, 1229–1242 (2018).
27. Doench, J. G. *et al.* Rational design of highly active sgRNAs for CRISPR-Cas9-mediated gene inactivation. *Nat. Biotechnol.* **32**, 1262–1267 (2014).
28. Kochenderfer, J. N., Yu, Z., Frasheri, D., Restifo, N. P. & Rosenberg, S. A. Adoptive transfer of syngeneic T cells transduced with a chimeric antigen receptor that recognizes murine CD19 can eradicate lymphoma and normal B cells. *Blood* **116**, 3875–3886 (2010).
29. Davila, M. L., Kloss, C. C., Gunset, G. & Sadelain, M. CD19 CAR-Targeted T Cells Induce Long-Term Remission and B Cell Aplasia in an Immunocompetent Mouse Model of B Cell Acute Lymphoblastic Leukemia. *PLoS One* **8**, 1–14 (2013).
30. Paszkiewicz, P. J. *et al.* Targeted antibody-mediated depletion of murine CD19 CAR T cells permanently reverses B cell aplasia. *J. Clin. Invest.* **126**, 4262–4272 (2016).
31. Boulch, M. *et al.* A cross-talk between CAR T cell subsets and the tumor microenvironment is essential for sustained cytotoxic activity. *Sci. Immunol.* **6**, 1–17 (2021).
32. Sotillo, E. *et al.* Convergence of acquired mutations and alternative splicing of CD19 enables resistance to CART-19 immunotherapy. *Cancer Discov.* **5**, 1282–1295 (2015).
33. Dufva, O. *et al.* Integrated drug profiling and CRISPR screening identify essential pathways for CAR T-cell cytotoxicity. *Blood* **135**, 597–609 (2020).
34. Creelan, B. C. & Antonia, S. J. The NKG2A immune checkpoint — a new direction in cancer immunotherapy. *Nat. Rev. Clin. Oncol.* **16**, 277–278 (2019).
35. Borst, L., van der Burg, S. H. & van Hall, T. The NKG2A-HLA-E axis as a novel checkpoint in the tumor microenvironment. *Clin. Cancer Res.* **26**, 5549–5556 (2021).
36. Braud, V. *et al.* HLA-E binds to natural killer cell receptors CD94/NKG2A, B and C. *Nature* **391**, 795–799 (1998).
37. Braud, V. M., Aldemir, H., Breart, B. & Ferlin, W. G. Expression of CD94-NKG2A inhibitory receptor is restricted to a subset of CD8+ T cells. *Trends Immunol.* **24**, 162–164 (2003).
38. Malmberg, K.-J. *et al.* IFN-γ protects short-term ovarian carcinoma cell lines from CTL lysis via a CD94/NKG2A-dependent mechanism. *J. Clin. Invest.* **110**, 1515–1523 (2002).
39. Le Dréan, E. *et al.* Inhibition of antigen-induced T cell response and antibody-induced NK cell cytotoxicity by NKG2A: Association of NKG2A with SHP-1 and SHP-2 protein-tyrosine phosphatases. *Eur. J. Immunol.* **28**, 264–276 (1998).
40. Anfossi, N. *et al.* Human NK Cell Education by Inhibitory Receptors for MHC Class I. *Immunity* **25**, 331–342 (2006).
41. André, P. *et al.* Anti-NKG2A mAb Is a Checkpoint Inhibitor that Promotes Anti-tumor Immunity by Unleashing Both T and NK Cells. *Cell* **175**, 1731-1743.e13 (2018).
42. van Montfoort, N. *et al.* NKG2A Blockade Potentiates CD8 T Cell Immunity Induced by Cancer Vaccines. *Cell* **175**, 1744-1755.e15 (2018).
43. Ruggeri, L. *et al.* Effects of anti-NKG2A antibody administration on leukemia and normal hematopoietic cells. *Haematologica* **101**, 626–633 (2016).

1146 44. Jain, M. D. *et al.* Tumor interferon signaling and suppressive myeloid cells are associated with CAR T-cell failure in large B-cell lymphoma. *Blood* **137**, 2621–2633 (2021).

1148 45. Benci, J. L. *et al.* Opposing Functions of Interferon Coordinate Adaptive and Innate Immune Responses to Cancer Immune Checkpoint Blockade. *Cell* **178**, 933-948.e14
1150 (2019).

46. Benci, J. L. *et al.* Tumor Interferon Signaling Regulates a Multigenic Resistance Program
1152 to Immune Checkpoint Blockade. *Cell* **167**, 1540-1554.e12 (2016).

47. Restifo, N. P. *et al.* Loss of Functional Beta2-Microglobulin in Metastatic Melanomas
1154 From Five Patients Receiving Immunotherapy. *JNCI J. Natl. Cancer Inst.* **88**, 100–108 (1996).

1156 48. Zaretsky, J. M. *et al.* Mutations associated with acquired resistance to PD-1 blockade in melanoma. *N. Engl. J. Med.* **375**, 819–829 (2016).

1158 49. Sade-Feldman, M. *et al.* Resistance to checkpoint blockade therapy through inactivation of antigen presentation. *Nat. Commun.* **8**, (2017).

1160 50. Sucker, A. *et al.* Acquired IFNγ resistance impairs anti-tumor immunity and gives rise to T-cell-resistant melanoma lesions. *Nat. Commun.* **8**, 1–15 (2017).

1162 51. Hart, T. *et al.* High-Resolution CRISPR Screens Reveal Fitness Genes and Genotype-Specific Cancer Liabilities. *Cell* **163**, 1515–1526 (2015).

1164 52. Doench, J. G. Am i ready for CRISPR? A user's guide to genetic screens. *Nat. Rev. Genet.* **19**, 67–80 (2018).

1166 53. Patro, R., Duggal, G., Love, M. I., Irizarry, R. A. & Kingsford, C. Salmon provides fast and bias-aware quantification of transcript expression. *Nat. Methods* **14**, 417–419 (2017).

1168 54. Soneson, C., Love, M. I. & Robinson, M. D. Differential analyses for RNA-seq: transcript-level estimates improve gene-level inferences. *F1000Research* **4**, 1521 (2016).

1170 55. Raghavan, S. *et al.* Microenvironment drives cell state, plasticity, and drug response in pancreatic cancer. *Cell* **184**, 6119-6137.e26 (2021).

1172 56. Tirosh, I. *et al.* Dissecting the multicellular ecosystem of metastatic melanoma by single-cell RNA-seq. *Science (80-.).* **352**, 189–196 (2016).

1174 57. Eyquem, J. *et al.* Targeting a CAR to the TRAC locus with CRISPR/Cas9 enhances tumour rejection. *Nature* **543**, 113–117 (2017).

1176 58. Posey, A. D. *et al.* Engineered CAR T Cells Targeting the Cancer-Associated Tn-Glycoform of the Membrane Mucin MUC1 Control Adenocarcinoma. *Immunity* **44**, 1444–
1178 1454 (2016).

59. Engels, B. *et al.* Retroviral Vectors for High-Level Transgene Expression in T
1180 Lymphocytes. *Hum. Gene Ther.* **14**, 1155–1168 (2003).

60. Morgan, R. A. *et al.* Recognition of glioma stem cells by genetically modified T cells
1182 targeting EGFRvIII and development of adoptive cell therapy for glioma. *Hum. Gene Ther.* **23**, 1043–1053 (2012).

1184 61. R Core Team. R: A Language and Environment for Statistical Computing. [online] Vienna, Austria: R Foundation for Statistical Computing. Available at [https://www.R-project.org].